Excitation of giant electric isovector resonances in pion charge exchange reactions

N. Auerbach
Los Alamos National Laboratory, Los Alamos, New Mexico 87545
and Department of Physics and Astronomy, Tel Aviv University, Tel Aviv 69978, Israel

Amir Klein
Department of Physics and Astronomy, Tel Aviv University, Tel Aviv 69978, Israel
and Soreq Nuclear Research Centre, Yavne 70600, Israel

(Received 9 May 1983)

Pion single charge-exchange reactions exciting giant electric isovector resonances are studied for a series of nuclei. The reaction mechanism is treated in the distorted-wave impulse approximation. Emphasis is put on the nuclear structure aspects probed in these reactions. Transition densities for charge-exchange excitations are calculated using the sum-rule method and microscopically, in the Hartree-Fock—random-phase-approximation framework. The resulting cross sections are sensitive to the nuclear structure input. Double differential cross sections as functions of the nuclear excitation energy are calculated.

[NUCLEAR REACTIONS Pion single charge exchange exciting giant isovector resonances.]

I. INTRODUCTION

Considerable experimental and theoretical[1,2] effort has been devoted in the past to the study of pion single charge exchange reactions. However, almost all of the studies were concerned with the excitation of the isobaric analog states.

In recent years, new experimental developments[3] have opened the possibility to study, in addition to the isobaric analog, other excited states. In particular, an experimental program was undertaken in order to study giant isovector resonances excited in $(\pi^{\pm},\pi^0)$ reactions. The observation of the charge-exchange components of the isovector dipole and monopole, for a series of nuclei, using incoming pions with $T_{\pi^{\pm}}=165$ MeV, has been reported.[4,5]

The $(\pi^{\pm},\pi^0)$ reactions, performed under the same kinematic conditions, promise to contribute significantly to our understanding of the differing roles played by the proton and neutron degrees of freedom in the charge exchange process. Information on the Coulomb polarization of the protons can be inferred from the cross sections in $N=Z$ nuclei, as shown in Ref. 6. In $N>Z$ nuclei, the pion charge exchange cross sections are expected to reflect the influence of the excess neutrons. The excess neutrons increase the number of configurations excited in the (π^+,π^0) process. Also, due to the Pauli principle, they exclude configurations which, otherwise, would have been excited in the (π^-,π^0) process.

The aim of this work is to present the results of a systematic study of the $(\pi^{\pm},\pi^0)$ reactions in which giant electric resonances of multipolarity 0^+, 1^-, and 2^+ are excited. We will describe the reaction mechanism in terms of the distorted-wave impulse approximation (DWIA). In this work, we will mainly deal with the aspects of nuclear structure of the problem. The relevant nuclear structure information will be derived in terms of the charge exchange Hartree-Fock—random phase approximation (HF-RPA) framework.[7] The cross sections will be calculated using transition densities derived both in the sum-rule method and, directly, from the RPA Green's function. The latter is equivalent to a calculation of the cross section in which the response of the nucleus to the pionic probe, namely the product of the incoming and outgoing pions distorted wave functions and the pion-nucleon t matrix, is evaluated. This method will enable us to obtain the double differential cross section as a function of the nuclear excitation energy. The calculated double differential cross sections can be directly compared with the type of data obtained in experiment.

We should stress here the general nature of the methods mentioned above. These can be applied to charge exchange reactions involving nucleons, light ions, and other kinds of mesons, such as kaons.

II. THE PION DWIA

The most commonly used approach to describe pion single charge-exchange reactions is the DWIA.[8] In this approximation, one assumes that the charge-exchange process between the initial and final nuclear states occurs only once during the multiple scattering sequence. The pion initial and final wave functions are distorted by the elastic pion nucleus optical potential, derived from the elementary pion-nucleon t matrix.

Let $|0\rangle$ denote the nuclear ground state, and $|n_\mu\rangle$ the state excited in a charge-exchange reaction involving $\Delta T_Z=\mu=\pm 1$. The DWIA transition amplitude between

the states $|0\rangle$, $|n_\mu\rangle$ is proportional to

$$T_{n_\mu 0}\sim\langle n_\mu|\int d^3\vec{r}\,d^3\vec{r}\,'\chi^{(-)*}(E',\vec{r}\,')\times\sum_{i=1}^{A}t(\vec{r},\vec{r}\,',\vec{r}_i)\chi^{(+)}(E,\vec{r})|0\rangle\quad(\mu=\pm1)\,, \tag{2.1}$$

where $\chi^{(+)}(E,\vec{r})$ and $\chi^{(-)}(E',\vec{r}\,')$ are the incoming and outgoing pion distorted waves, respectively, and $t(\vec{r},\vec{r}\,',\vec{r}_i)$ is the pion-nucleon t matrix. The distorted waves are calculated by solving the Klein-Gordon equation with an optical potential, $V_{\rm opt}$. In the lowest order DWIA, this optical potential is determined as follows:

$$V_{\rm opt}(\vec{r},\vec{r}\,')\sim\left\langle 0\left|\sum_{i=1}^{A}t(\vec{r},\vec{r}\,',\vec{r}_i)\right|0\right\rangle\,. \tag{2.2}$$

The pion-nucleon t matrix can be generally written as the following:

$$t(\vec{r},\vec{r}\,',\vec{r}_i)=t_s(\vec{r},\vec{r}\,',\vec{r}_i)+\vec{\tau}\cdot\vec{I}_\pi t_v(\vec{r},\vec{r}\,',\vec{r}_i)\,. \tag{2.3}$$

In Eq. (2.3) $\vec{\tau}$ is the nucleon Pauli isospin and $\vec{I}_\pi$ is the pion isospin. Both quantities t_s,t_v enter in the calculation of $V_{\rm opt}$, but, for charge-exchange reactions, only t_v enters into the transition amplitude. General arguments lead to the following expressions for t_s,t_v in the momentum space:

$$t_s(\vec{k},\vec{k}\,')=\alpha_1^s+\alpha_2^s\vec{k}\cdot\vec{k}\,'-\alpha_3^s(\vec{k}-\vec{k}\,')^2+\alpha_4^s\vec{k}^{\,2}+\alpha_5^s\vec{k}\,'^2\,, \tag{2.4}$$

$$t_v(\vec{k},\vec{k}\,')=\alpha_1^v+\alpha_2^v\vec{k}\cdot\vec{k}\,'-\alpha_3^v(\vec{k}-\vec{k}\,')^2+\alpha_4^v\vec{k}^{\,2}+\alpha_5^v\vec{k}\,'^2\,, \tag{2.5}$$

where $\vec{k},\vec{k}\,'$ are the incoming and outgoing pions momenta, respectively, and the coefficients α_i^s,α_i^v $(i=1,\ldots,5)$ are functions of the pion-nucleon phase shifts. It has been shown[8] that the above-mentioned forms for t_s,t_v give rise to a (lowest order) optical potential which depends on the isoscalar and isovector nuclear ground state densities. For the non-spin-flip pion charge-exchange transition amplitude, one can derive[1,8] the following expression:

$$T_{n_\mu 0}\sim\int d^3\vec{r}\,\chi^{(-)*}(E',\vec{r})\{\gamma_1\rho_{n_\mu}(\vec{r})+\gamma_2[\vec{\nabla}^2\rho_{n_\mu}(\vec{r})]+\gamma_3\overleftarrow{\nabla}\rho_{v_\mu}(\vec{r})\vec{\nabla}+\gamma_4\overleftarrow{\nabla}^2\rho_{n_\mu}(\vec{r})\}\chi^{(+)}(E,\vec{r})\,, \tag{2.6}$$

where the isovector transition density $\rho_{n_\mu}(\vec{r})$ is defined as follows:

$$\rho_{n_\mu}(\vec{r})=\left\langle n_\mu\left|\sum_{i=1}^{A}\delta(\vec{r}-\vec{r}_i)\tau_\mu(i)\right|0\right\rangle \tag{2.7}$$

and

$$\tau_\mu=\begin{cases}\tau_z & \mu=0\\ \mp\dfrac{1}{\sqrt{2}}(\tau_x\pm i\tau_y) & \mu=\pm1\,.\end{cases} \tag{2.8}$$

In Eq. (2.6), $\vec{\nabla}$ acts to the right, $\overleftarrow{\nabla}$ acts to the left. The coefficients γ_i, $i=1,\ldots,4$, depend on the pion-nucleon phase shifts and on the off-shell model used for the t matrix.

III. NUCLEAR STRUCTURE

A. General considerations

The basic element of the nuclear structure relevant to any pion single charge exchange theory is the isovector transition density. Transition densities for isoscalar and the $\Delta T_z=0$ component of isovector electric resonances were calculated in the past using macroscopic models,[9–13] the sum-rule method,[14–17] and the microscopic approaches.[18–23]

The transition densities for the $\Delta T_z=\pm1$ excitations should incorporate nuclear structure effects that play a role in such modes: the violation of charge independence, due to the Coulomb interaction, Pauli blocking due to the excess neutrons (in $N>Z$ nuclei), different energetics, and different (escape and spreading) widths in the two final nuclei reached in the charge-exchange process. We will obtain the quantity defined in Eq. (2.7), using the HF-RPA framework.

B. The nuclear response and the HF-RPA framework

The linear response approach has proved to be a powerful tool in the description of giant isoscalar and isovector electric excitations,[19,20] magnetic states,[24,25] and μ^- capture rates.[26] It has recently been applied in a systematic study of the charge-exchange components of giant electric isovector resonances.[7]

Let Q_μ be a one body operator proportional to τ_μ. The transition strength of Q_μ is calculated by examining the residues at the positive poles of the expression

$$S_\mu(E)=\frac{1}{\pi}\,\mathrm{Im}\,\mathrm{Tr}[Q_\mu^\dagger G_\mu(E)Q_\mu]\,, \tag{3.1}$$

where $G_\mu(E)$ is the particle-hole Green's function at excitation energy E. The precise definitions[7] are the following:

$$G_{+1}(x_1,x_2,x_1',x_2',E)=2\sum_{n_{+1},\eta\to0^+}\frac{\langle0|\psi_{\rm p}^\dagger(x_1)\psi_{\rm n}(x_2)|n_{+1}\rangle\langle n_{+1}|\psi_{\rm n}^\dagger(x_1')\psi_{\rm p}(x_2')|0\rangle}{E_{n_{+1}}-E-i\eta}+2\sum_{n_{-1},\eta\to0^+}\frac{\langle0|\psi_{\rm n}^\dagger(x_1')\psi_{\rm p}(x_2')|n_{-1}\rangle\langle n_{-1}|\psi_{\rm p}^\dagger(x_1)\psi_{\rm n}(x_2)|0\rangle}{E_{n_{-1}}+E-i\eta}\,, \tag{3.2}$$

$$G_{-1}(x_1,x_2,x_1',x_2',E)=2\sum_{n_{-1},\eta\to 0^+}\frac{\langle 0|\psi_n^\dagger(x_1)\psi_p(x_2)|n_{-1}\rangle\langle n_{-1}|\psi_p^\dagger(x_1')\psi_n(x_2')|0\rangle}{E_{n_{-1}}-E-i\eta}$$
$$+2\sum_{n_{+1},\eta\to 0^+}\frac{\langle 0|\psi_p^\dagger(x_1')\psi_n(x_2')|n_{+1}\rangle\langle n_{+1}|\psi_n^\dagger(x_1)\psi_p(x_2)|0\rangle}{E_{n_{+1}}+E-i\eta}\ , \tag{3.3}$$

$$G_0(x_1,x_2,x_1',x_2',E)=\sum_{n_0,\eta\to 0^+}\frac{\langle 0|\psi^\dagger(x_1)\psi(x_2)|n_0\rangle\langle n_0|\psi^\dagger(x_1')\psi(x_2')|0\rangle}{E_{n_0}-E-i\eta}$$
$$+\frac{\langle 0|\psi^\dagger(x_1'\psi(x_2')|n_0\rangle\langle n_0|\psi^\dagger(x_1)\psi(x_2)|0\rangle}{E_{n_0}+E-i\eta}\ , \tag{3.4}$$

where $\psi_p^\dagger(x)$, $\psi_p(x)$ are the creation and annihilation operators of a proton at the point x (x includes spin), $\psi_n^\dagger(x)$, $\psi_n(x)$ are analogous operators for a neutron, $\psi=\psi_n-\psi_p$, and E_{n_μ} is the excitation energy of the state $|n_\mu\rangle$. We work in a HF representation. The particle-hole Green's function can be obtained by solving the ladder approximation equation, which we write schematically as follows:

$$G_\mu(E)=G_\mu^{(0)}(E)-G_\mu^{(0)}(E)\Gamma(E)G_\mu(E)\ , \tag{3.5}$$

where $G_\mu^{(0)}(E)$ is the free particle-hole Green's function and $\Gamma(E)$ is the particle-hole interaction. In the HF-RPA self-consistent framework, this interaction equals the second derivative of the HF energy with respect to one-body densities,[19,27] and the calculations are performed in a complete 1p-1h space. In Ref. 7 it was shown that the following sum rules hold in the self-consistent charge-exchange framework, provided Q_μ is energy independent:

$$\sum_{n_{-1}}|\langle n_{-1}|Q_{-1}|0\rangle|^2-\sum_{n_{+1}}|\langle n_{+1}|Q_{+1}|0\rangle|^2=\langle\phi_0|[Q_{+1},Q_{-1}]|\phi_0\rangle\ \text{(NEWSR)}\ , \tag{3.6}$$

$$\sum_{n_{-1}}E_{n_{-1}}|\langle n_{-1}|Q_{-1}|0\rangle|^2+\sum_{n_{+1}}E_{n_{+1}}|\langle n_{+1}|Q_{+1}|0\rangle|^2=\langle\phi_0|[Q_{+1},[H,Q_{-1}]]|\phi_0\rangle\ \text{(EWSR)}\ , \tag{3.7}$$

where H is the total Hamiltonian and $|\phi_0\rangle$ is the HF ground state wave function. These Thouless-type sum rules can be straightforwardly generalized for any one body energy independent operators, P_μ, Q_μ, as follows:

$$\sum_{n_{-1}}\langle 0|P_{+1}|n_{-1}\rangle\langle n_{-1}|Q_{-1}|0\rangle-\sum_{n_{+1}}\langle 0|Q_{-1}|n_{+1}\rangle\langle n_{+1}|P_{+1}|0\rangle=\langle\phi_0|[P_{+1},Q_{-1}]|\phi_0\rangle\ , \tag{3.8}$$

$$\sum_{n_{-1}}E_{n_{-1}}\langle 0|P_{+1}|n_{-1}\rangle\langle n_{-1}|Q_{-1}|0\rangle+\sum_{n_{+1}}E_{n_{+1}}\langle 0|Q_{-1}|n_{+1}\rangle\langle n_{+1}|P_{+1}|0\rangle=\langle\phi_0|[P_{+1},[H,Q_{-1}]]|\phi_0\rangle\ . \tag{3.9}$$

C. Transition densities from the sum-rule method

The starting points of the method[28] are Eqs. (3.8) and (3.9). For transitions which involve no spin flip, we can substitute the following:

$$Q_\mu^{(L)}=\sum_{i=1}^{A}f_L(r_i)Y_{LM}(\hat{r}_i)\tau_\mu(i)\ , \tag{3.10}$$

$$P_\mu^{(L)}(\vec{r})=\sum_{i=1}^{A}\frac{\delta(r-r_i)}{rr_i}Y_{LM}^*(\hat{r})Y_{LM}(\hat{r}_i)\tau_\mu(i)\ . \tag{3.11}$$

$Q_\mu^{(L)}$ is an operator which excites electric isovector resonances of multipolarity L and $P_\mu^{(L)}(\vec{r})$ is the μ component of the corresponding transition density. Assuming that we deal with spherical nuclei, we obtain from Eq. (3.8),

$$\sum_{n_{-1}}R_{n_{-1}}^{(L)}\rho_{n_{-1}}^{(L)}(r)-\sum_{n_{+1}}R_{n_{+1}}^{(L)}\rho_{n_{+1}}^{(L)}(r)=2f_L(r)[\rho_n(r)-\rho_p(r)]\ , \tag{3.12}$$

where

$$R_{n_\mu}^{(L)}=\langle n_\mu|Q_\mu^{(L)}|0\rangle \tag{3.13}$$

and $\rho_{n_\mu}^{(L)}(r)$ is the radial part of the transition density, i.e.,

$$\langle n_\mu|P_\mu^{(L)}(\vec{r})|0\rangle=\rho_{n_\mu}^{(L)}(r)Y_{LM}^*(\hat{r})\ . \tag{3.14}$$

Also, $\rho_n(r)$ and $\rho_p(r)$ are the ground state (HF) density distributions of neutrons and protons, respectively. It is worthwhile mentioning that (i) Eq. (3.12) holds also for the charge-exchange TDA, (ii) the specific form of the particle-hole interaction is not important for its validity, and (iii) the only necessary requirement for Eq. (3.12) to hold is that the 1p-1h space be complete.

Substituting $P_\mu^{(L)}$, $Q_\mu^{(L)}$ of Eqs. (3.10) and (3.14) into Eq. (3.9) we obtain the following:

$$\sum_{n_{-1}} E_{n_{-1}} R^{(L)}_{n_{-1}} \rho_{n_{-1}}(r) + \sum_{n_{+1}} E_{n_{+1}} R^{(L)}_{n_{+1}} \rho_{n_{+1}}(r) = \frac{\hbar^2}{m} \left\{ \rho(r) \left[-\frac{1}{r}\frac{df_L(r)}{dr} + L(L+1)\frac{f_l(r)}{r^2} \right] - \frac{d}{dz}\left[\frac{z}{r}\frac{df_L(z)}{dz}\rho(z) \right]_{z=r} \right\}$$

$$+ \langle \phi_0 | [P^{(L)}_{+1}, [V_{\text{exch}}, Q^{(L)}_{-1}]] | \phi_0 \rangle + 2V_c(r) f_L(r) [\rho_n(r) - \rho_p(r)] , \quad (3.15)$$

V_{exch} is the exchange part of the nucleon-nucleon force, $V_c(r)$ is the Coulomb potential, and $\rho(r)$ denotes the HF ground state density.

We should mention that Eq. (3.15) holds only in the self-consistent RPA framework. Adopting a Skyrme-type[29] two body force, we can express the second term on the rhs of Eq. (3.15) as follows:

$$\langle \phi_0 | [P^{(L)}_{+1}, [V_{\text{exch}}, Q^{(L)}_{-1}]] | \phi_0 \rangle = \tfrac{1}{2}(t_1 + t_2) \left\{ g(r) \left[-\frac{1}{r}\frac{df_L(r)}{dr} + L(L+1)\frac{f_L(r)}{r^2} \right] - \frac{d}{dz}\left[\frac{z}{r}\frac{df_L(z)}{dz} g(z) \right]_{z=r} \right\} , \quad (3.16)$$

where t_1, t_2 are the coefficients of the velocity-dependent parts of the Skyrme force and

$$g(r) = 4\rho_n(r)\rho_p(r) + \tfrac{1}{2}[\rho_n(r) - \rho_p(r)]^2 . \quad (3.17)$$

Notice that if we multiply Eqs. (3.12) and (3.15) by $Y^*_{LM}(r) f_L(r) Y_{LM}(r)$ and perform an integration over the nuclear volume, we obtain the non-energy-weighted sum rule (NEWSR) and energy-weighted sum rule (EWSR) of Ref. 7

$$\sum_{n_{-1}} S^{(L)}_{n_{-1}} - \sum_{n_{+1}} S^{(L)}_{n_{+1}} = \frac{1}{2\pi}[N\langle f_L^2(r)\rangle_n - Z\langle f_L^2(r)\rangle_p] , \quad (3.18)$$

$$\sum_{n_{-1}} E_{n_{-1}} S^{(L)}_{n_{-1}} + \sum_{n_{+1}} E_{n_{+1}} S^{(L)}_{n_{+1}} = \frac{\hbar^2}{m}\frac{1}{4\pi} A \left\langle \left[\frac{df_L(r)}{dr} \right]^2 + L(L+1)\frac{f_L^2(r)}{r^2} \right\rangle (1+\kappa+\eta) , \quad (3.19)$$

where

$$S^{(L)}_{n_\mu} = R^{(L)2}_{n_\mu} = \langle n_\mu | Q^{(L)}_\mu | 0 \rangle^2$$

is the transition strength to the RPA state $|n_\mu\rangle$ and all other notations are identical to those of Ref. 7.

After the derivation of Eqs. (3.12), (3.15), and (3.16), the next step is to apply the closure approximation, i.e., to replace the sum over $|n_\mu\rangle$ by a single term, containing the total strength $S^{(L)}_\mu$, where

$$S^{(L)}_\mu = \sum_{n_\mu} S^{(L)}_{n_\mu} , \quad (3.20)$$

and the average excitation energy, defined as

$$E^{(L)}_\mu = \frac{\sum_{n_\mu} E_{n_\mu} S^{(L)}_{n_\mu}}{S^{(L)}_\mu} . \quad (3.21)$$

We obtain

$$R^{(L)}_{-1}\rho^{(L)}_{-1}(r) - R^{(L)}_{+1}\rho^{(L)}_{+1}(r) = 2f_L(r)[\rho_n(r) - \rho_p(r)] , \quad (3.22)$$

$$E^{(L)}_{-1}R^{(L)}_{-1}\rho^{(L)}_{-1}(r) + E^{(L)}_{+1}R^{(L)}_{+1}\rho^{(L)}_{+1}(r) = \text{rhs of Eq. (3.15)}, \quad (3.23)$$

where $R^{(L)2}_\mu = S^{(L)}_\mu$. The quantities $\rho^{(L)}_{\pm 1}(r)$ are obtained by solving Eqs. (3.22) and (3.23). [The procedure described in Eqs. (3.10)—(3.22) can be carried out also for spin-flip transitions.] We remark that the closure approximation may be applied for the isovector dipole and quadrupole, where the strengths of all three modes are fairly well concentrated.[7] In the case of the monopole the $\Delta T_z = -1$ component induced by

$$Q^{(0)}_\mu = \sum_{i=1}^{A} r_i^2 Y_{00} \tau^{(i)}_\mu$$

has two comparable concentrations of strength: the isobaric analog resonance[7] (IAR) at the lower energy end and the isovector monopole at the higher energy end; these are separated by a rather large energy interval. We can take this fact into account by explicitly introducing into Eqs. (3.22) and (3.23) the known[30] transition density and energy for the IAR, $\rho(r)^{(\text{IAR})}$ and $E^{(\text{IAR})}$ leaving the transition density for the monopole, $\rho^{(M)}_{-1}(r)$ to be determined. We use

$$\rho^{(\text{IAR})}(r) = \left[\frac{8\pi}{N-Z} \right]^{1/2} \rho_{\text{excess}}(r) , \quad (3.24)$$

where $\rho_{\text{excess}}(r)$ is the density of the excess neutrons. The normalization is chosen so that

$$| \langle \text{IAR} | \sum_{i=1}^{A} \tau_{-1}(i) | 0 \rangle |^2 = 2(N-Z) . \quad (3.25)$$

For the energy $E^{(\text{IAR})}$ we use the experimental Coulomb displacement energy.[31] The transition densities derived from the sum rules, with

$$f_L(r)=\begin{cases} r^2 & L=0 \\ r^L & L\neq 0 \end{cases}, \tag{3.26}$$

turn out to be the following:

For the charge-exchange monopole,

$$\rho_\mu^{(M)}(r)=-\frac{2\hbar^2}{m}\left[3\rho(r)+r\frac{d\rho(r)}{dr}\right]-(t_1+t_2)\left[3g(r)+r\frac{dg(r)}{dr}\right]+\frac{2r^2[\rho_n(r)-\rho_p(r)][V_c(r)-\mu E_{-\mu}^{(M)}]-2r_{\text{excess}}^2\rho_{\text{excess}}(r)(E^{(\text{IAR})}-\mu E_{-\mu}^{(M)})}{R_\mu^{(M)}(E_{-1}^{(M)}+E_{+1}^{(M)})} \tag{3.27}$$

where $S_\mu^{(M)}$ is the transition strength of the monopole, $R_\mu^{(M)2}=S_\mu^{(M)}$, and

$$r_{\text{excess}}^2=\frac{1}{N-Z}\int d^3\vec{r}\,r^2\rho_{\text{excess}}(r)\ . \tag{3.28}$$

For the charge-exchange dipole,

$$\rho_\mu^{(1)}(r)=\frac{-\frac{\hbar^2}{m}\frac{d\rho(r)}{dr}-\frac{1}{2}(t_1+t_2)\frac{dg(r)}{dr}+2r[\rho_n(r)-\rho_p(r)][V_c(r)-\mu E_{-\mu}^{(1)}]}{R_\mu^{(1)}(E_{-1}^{(1)}+E_{+1}^{(1)})}\ . \tag{3.29}$$

For the charge-exchange quadrupole,

$$\rho_\mu^{(2)}(r)=\frac{-\frac{2\hbar^2}{m}r\frac{d\rho(r)}{dr}-(t_1+t_2)r\frac{dg(r)}{dr}+2r^2[\rho_n(r)-\rho_p(r)][V_c(r)-\mu E_{-\mu}^{(2)}]}{R_\mu^{(2)}(E_{-1}^{(2)}+E_{+1}^{(2)})}\ . \tag{3.30}$$

The first term in the numerator on the rhs of Eqs. (3.27), (3.29), and (3.30) (which we will refer to as the *Tassie term*) represents the contribution of the kinetic energy of the nuclear Hamiltonian to the double commutator, and it is identical in its shape with the transition density for isoscalar excitations deduced from nuclear collective models,[9] or from the classical oscillator sum rule.[36] The term proportional to (t_1+t_2) comes from the exchange part of the nucleon-nucleon force,[29] and we will refer to it as the *exchange term*. The third term in Eqs. (3.27), (3.29), and (3.30) is responsible for the difference in the shapes of the transition densities for the $\mu=-1$ and $\mu=+1$ modes. (In $N=Z$ nuclei, this term is a direct consequence of the violation of charge independence as probed by an isovector operator.) The term proportional to $\rho_n(r)-\rho_p(r)$ in Eqs. (3.29) and (3.30) will be referred to as the *symmetry term*. In the monopole case, the symmetry term will include also the term proportional to $\rho_{\text{excess}}(r)$, which is a result of the subtraction of the IAR.

D. Microscopic transition densities

The transition density $\rho_{n_\mu}^{(L)}(r)$ can be calculated in the linear response approach using the following formula:

$$\rho_{n_\mu}^{(L)}(r)=\pm\left\{\frac{1}{\pi}\text{Im Tr}[U_\mu^{(L)\dagger}(r)G_\mu(E_{n_\mu})U_\mu^{(L)}(r)]\right\}^{1/2}, \tag{3.31}$$

where [see Eq. (3.11)]

$$U_\mu^{(L)}(r)=\sum_{i=1}^{A}\frac{\delta(r-r_i)}{rr_i}Y_{LM}(\hat{r}_i)\tau_\mu(i)\ . \tag{3.32}$$

The sign of $\rho_{n_\mu}^{(L)}(r)$ cannot be determined from Eq. (3.31), but it may be guessed by using

$$|\langle n_\mu|Q_\mu^{(L)}|0\rangle|^2=\left[\int d^3\vec{r}\,Q_\mu^{(L)}(\vec{r})\rho_{n_\mu}^{(L)}(r)Y_{LM}^*(r)\right]^2 \tag{3.33}$$

[see Eq. (3.10)], and also, by assuming that it resembles the shape of a phenomenologically derived $\rho_{n_0}^{(L)}(r)$. In order to avoid the ambiguities and the difficulties in determining the sign of $\rho_{n_\mu}^{(L)}(r)$ in Eq. (3.31), we use the following alternative approach: the transition density is obtained from the off-diagonal response, rather than from the diagonal one, as in Eq. (3.31). The formula is

$$\rho_{n_\mu}^{(L)}(r)=\frac{\langle 0|Q_\mu^{(L)\dagger}|n_\mu\rangle\langle n_\mu|U_\mu^{(L)}(r)|0\rangle}{\langle n_\mu|Q_\mu^{(L)}|0\rangle}=\frac{\frac{1}{\pi}\text{Im Tr}[Q_\mu^{(L)\dagger}G_\mu(E_{n_\mu})U_\mu^{(L)}(r)]}{R_{n_\mu}^{(L)}}\ , \tag{3.34}$$

where $R_{n_\mu}^{(L)}$ was defined in Eq. (3.13). The sign of $\rho_{n_\mu}^{(L)}(r)$ as calculated from Eq. (3.34) is no longer arbitrary; also, the normalization, Eq. (3.33), follows automatically.

IV. RESULTS FOR STRENGTHS AND TRANSITION DENSITIES

A. RPA results

The HF basis is obtained by using the Skyrme III force.[29] The RPA equation (3.5) is solved in the r-coordinate space,[19] and the linear response to the one body operator $Q_\mu^{(L)}$ can be evaluated by

TABLE I. Properties of the ground states of the calculated nuclei.

Nucleus	Isospin	rms radii (fm) r_n (neutrons)	r_p (protons)	r_c (charge)	r	$\langle r^2_{excess}\rangle^{1/2}$
^{40}Ca	0	3.36	3.41	3.50	3.39	
^{48}Ca	4	3.60	3.47	3.56	3.54	4.10
^{60}Ni	2	3.79	3.77	3.85	3.78	4.28
^{90}Zr	5	4.31	4.26	4.34	4.29	4.90
^{120}Sn	10	4.76	4.65	4.72	4.71	5.15
^{140}Ce	12	4.98	4.89	4.96	4.94	5.42
^{208}Pb	22	5.65	5.53	5.58	5.60	6.10

$$S^{(L)}_{n_\mu}=\frac{1}{\pi}\mathrm{Im}\left[\int r^2 r'^2 f^*_L(r)G_\mu(r,r',E_{n_\mu})f_L(r')dr\,dr'\right] \tag{4.1}$$

[see also, Eq. (3.1)]. The 1p-1h continuum is taken into account using the method of Ref. 32, and, consequently, the calculations will render particle escape widths. The spreading widths are not treated in our framework; however, they are expected to be of the order of 2–4 MeV.[33] The inclusion of spreading widths into the calculations should not very much affect our results.

In Table I details are shown about the ground states of the calculated nuclei. For ^{40}Ca, $r_n < r_p$ due to the Coulomb polarization.[14,34,35] This effect is counterbalanced in the other nuclei, by the excess neutrons.

In Tables II–IV the calculated RPA strengths and average excitation energies [see Eqs. (3.20) and (3.21)] for the charge-exchange components of the monopole, dipole, and quadrupole are given. The operators for these excitations are defined in Eq. (3.26). The NEWSR and EWSR of Eqs. (3.18) and (3.19), respectively, are exhausted up to 83–95 % for all the nuclei treated, except ^{40}Ca. In this nucleus, we focus our attention on rather subtle effects, and hence, numerical accuracy is crucial. We used a final spacial mesh to solve the RPA equations for ^{40}Ca, and the sum rules are exhausted up to 95–100 %. The differences in $S^{(L)}_\mu$, $\mu=\pm1$, for $L=0$, 1, and 2 in ^{40}Ca are a consequence of the Coulomb polarization effect in the parent nucleus ground state, as may be seen from the NEWSR. In the other nuclei, $S^{(L)}_{+1}<S^{(L)}_{-1}$ for $L=1,2$ because the excess neutrons: (i) contribute to the $\Delta T_z=-1$ transitions and (ii) exclude some of the $\Delta T_z=+1$ type configurations (Pauli blocking). This blocking effect is most pronounced for the charge-exchange dipole in the heavier nuclei. With respect to the 0^+ case, part of the excess neutron transition strength goes to the IAR, and it may happen (in ^{90}Zr, for example) that $S^{(M)}_{+1}>S^{(M)}_{-1}$.

In ^{40}Ca, the average excitation energies for a given multipolarity are separated by about twice the Coulomb displacement energy, and in the other nuclei, this separation is reduced by the symmetry energy.[36]

As representative examples, we show in Figs. 1 and 2 the calculated distributions of strength for ^{40}Ca and ^{208}Pb. More details about the RPA results can be found in Ref. 7.

B. Results for transition densities: The sum-rule approach

The radial parts of the transition densities are calculated from Eqs. (3.27)–(3.29), by using the Skyrme III HF ground state densities and the RPA results of Tables II–IV. As examples, we show in Figs. 3–8 the results obtained for the $L=0$, 1, and 2 charge-exchange transitions in ^{40}Ca and ^{208}Pb. The total transition density for each mode, represented by a continuous line, is the sum of the three terms discussed in Sec. III C.

We observe that the calculated transition densities differ in their shapes from the Tassie term. This is due to the exchange and symmetry terms. In $N=Z$ nuclei the symmetry term contributes little to the total transition density; its effect is mainly felt at the tail of the transition density. However, it is this term that accounts for the Coulomb polarization in the parent nucleus ground state.[28] For nuclei which possess large values of $N-Z$, the situation is different: the symmetry term contributes substantially to the transition density. Finally, we observe that the transi-

TABLE II. RPA results for the total transition strengths and average excitation energies of the charge-exchange monopole.

Nucleus	$S^{(M)}_{+1}$ (fm^4)	$E^{(M)}_{+1}$ (MeV)	$S^{(M)}_{-1}$ (fm^4)	$E^{(M)}_{-1}$ (MeV)
^{40}Ca	127.3	26.0	88.9	42.6
^{48}Ca	105.7	33.0	155.9	38.7
^{60}Ni	127.7	25.9	204.0	41.4
^{90}Zr	400.0	22.9	377.0	42.3
^{120}Sn	431.7	22.4	859.4	39.6
^{140}Ce	590.2	21.8	959.6	42.8
^{208}Pb	1026.6	16.3	1997.4	43.5

TABLE III. RPA results for the total transition strengths and average excitation energies of the charge-exchange dipole.

Nucleus	$S^{(1)}_{+1}$ (fm^2)	$E^{(1)}_{+1}$ (MeV)	$S^{(1)}_{-1}$ (fm^2)	$E^{(1)}_{-1}$ (MeV)
^{40}Ca	13.1	13.0	12.0	27.8
^{48}Ca	6.0	17.4	24.2	23.4
^{60}Ni	12.0	11.9	23.6	26.2
^{90}Zr	17.6	8.2	44.8	26.4
^{120}Sn	10.2	6.5	84.2	25.6
^{140}Ce	4.5	8.0	105.1	26.6
^{208}Pb	2.3	6.9	204.0	28.1

TABLE IV. RPA results for the total transition strengths and average excitation energies of the charge-exchange quadrupole.

Nucleus	$S^{(2)}_{+1}$ (fm^4)	$E^{(2)}_{+1}$ (MeV)	$S^{(2)}_{-1}$ (fm^4)	$E^{(2)}_{-1}$ (MeV)
^{40}Ca	292.9	25.1	256.2	40.1
^{48}Ca	217.3	29.9	526.0	34.2
^{60}Ni	459.7	23.8	658.0	35.9
^{90}Zr	832.9	19.6	1431.8	36.6
^{120}Sn	1009.1	18.0	3202.6	33.8
^{140}Ce	1120.2	17.6	4012.0	35.7
^{208}Pb	1532.6	12.1	9636.2	36.1

tion densities for the Pauli blocked $\mu=+1$ modes in heavy nuclei have more than one node. This is not surprising. For example, one would expect the transition density for the 1^-, $\mu=+1$ excitation in ^{208}Pb to have nodes, since this excitation is due to $3\hbar\omega$ 1p-1h configurations.

C. Results for transition densities: The microscopic approach

The transition density for an excited state $|n_\mu\rangle$ at energy E_{n_μ} is directly evaluated with the RPA Green's function, $G_\mu(r,r',E_{n_\mu})$, in r-coordinate space, as follows:

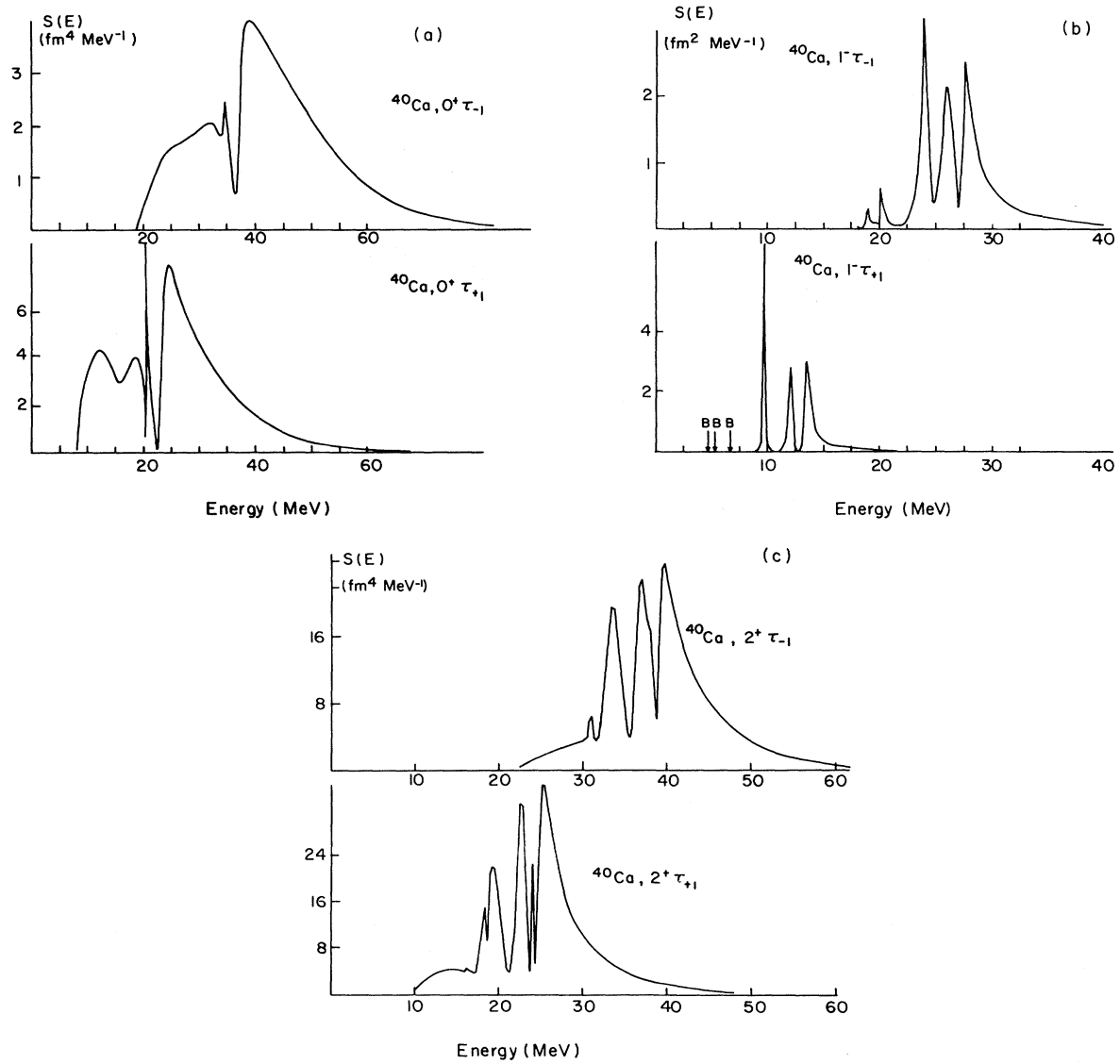

FIG. 1. Distributions of strength for the $\Delta T_z=\pm1$ components of the (a) monopole, (b) dipole, and (c) quadrupole in ^{40}Ca.

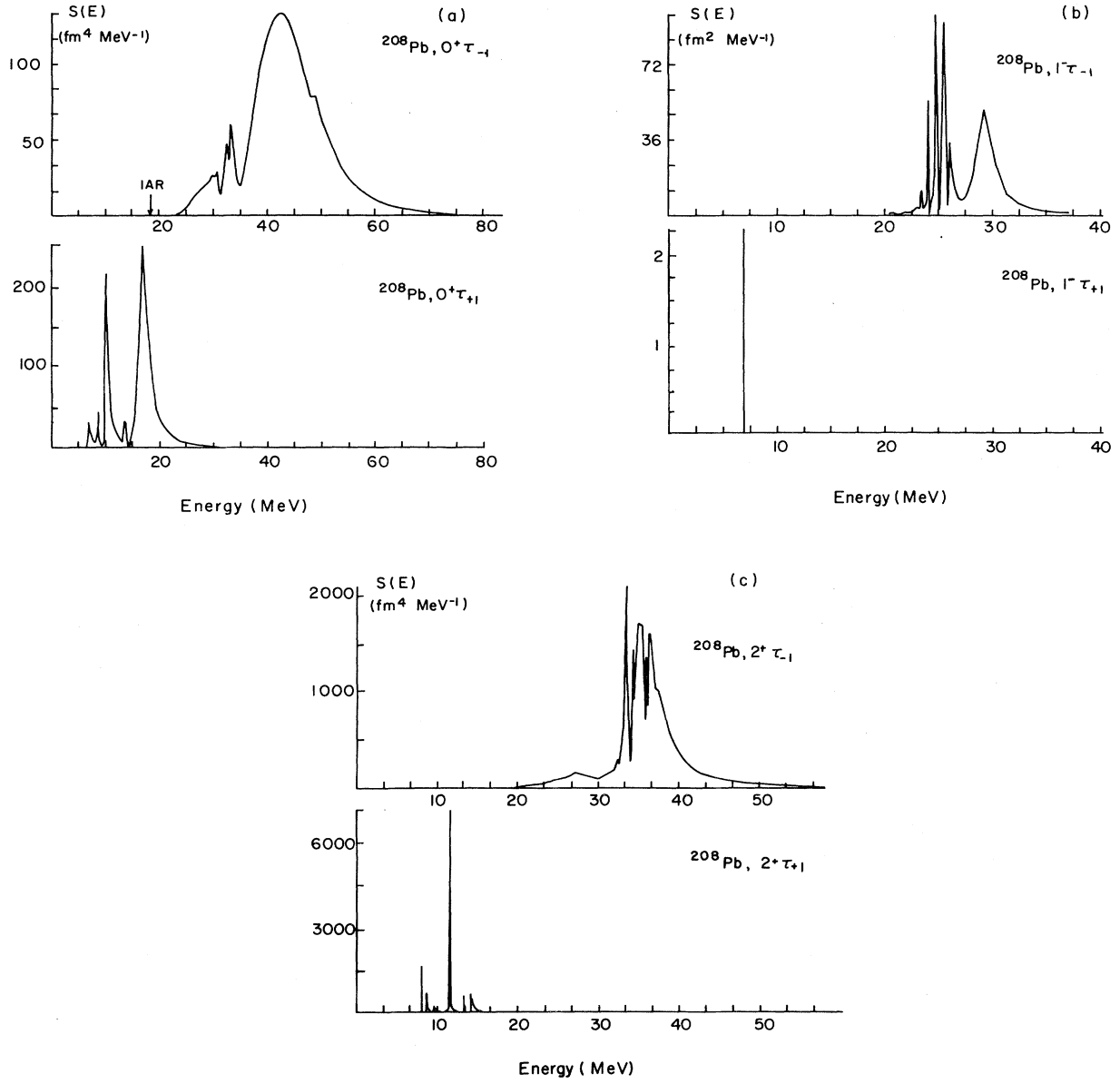

FIG. 2. Distributions of strength for the $\Delta T_z = \pm 1$ components of the (a) monopole, (b) dipole, and (c) quadrupole in ^{208}Pb.

$$\rho^{(L)}_{n_\mu}(r) = \frac{\frac{1}{\pi}\mathrm{Im}\left[\int r'^2 f_L^*(r') G_\mu(r', r, E_{m_\mu}) dr'\right]}{\left\{\frac{1}{\pi}\mathrm{Im}\left[\int r'^2 r''^2 f_L^*(r') G_\mu(r', r'', E_{n_\mu}) f_L(r'') dr' dr''\right]\right\}^{1/2}} ,$$

where $f_L(r)$ is given in Eq. (3.26).

We will discuss in detail the $\Delta T_z = \pm 1$ components of the dipole in ^{40}Ca. This case is interesting because the peaks are quite well separated, and it is possible to attach some physical meaning to each of them. The transition densities for the three main peaks are shown in Fig. 9. The peak at the lower energy end in both the $\Delta T_z = +1$ and $\Delta T_z = -1$ modes represents a volume transition, while the other two have the characteristics of a surface transition. Of course, the $\Delta T_z = +1$ transition density and its analogous $\Delta T_z = -1$ density differ little; we attribute this difference to the Coulomb polarization in the parent nucleus ground state as well as in the final (excited) state.[6]

In Figs. 10–14 the transition densities for the strongest peaks in the strength distributions of the charge-exchange monopole and quadrupole of ^{40}Ca, and monopole, dipole, and quadrupole of ^{208}Pb are shown. These transition den-

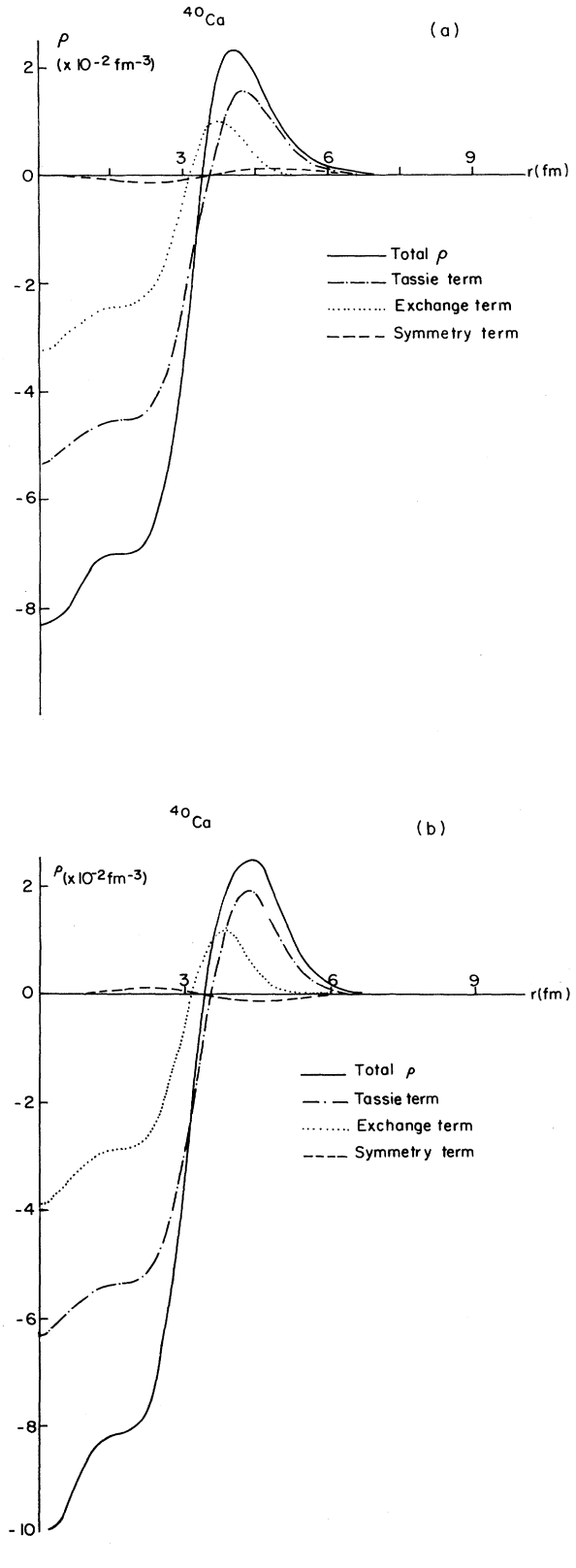

FIG. 3. The transition densities for the (a) $\Delta T_z = +1$ and (b) $\Delta T_z = -1$ modes of the monopole in ^{40}Ca, calculated using the sum-rule method.

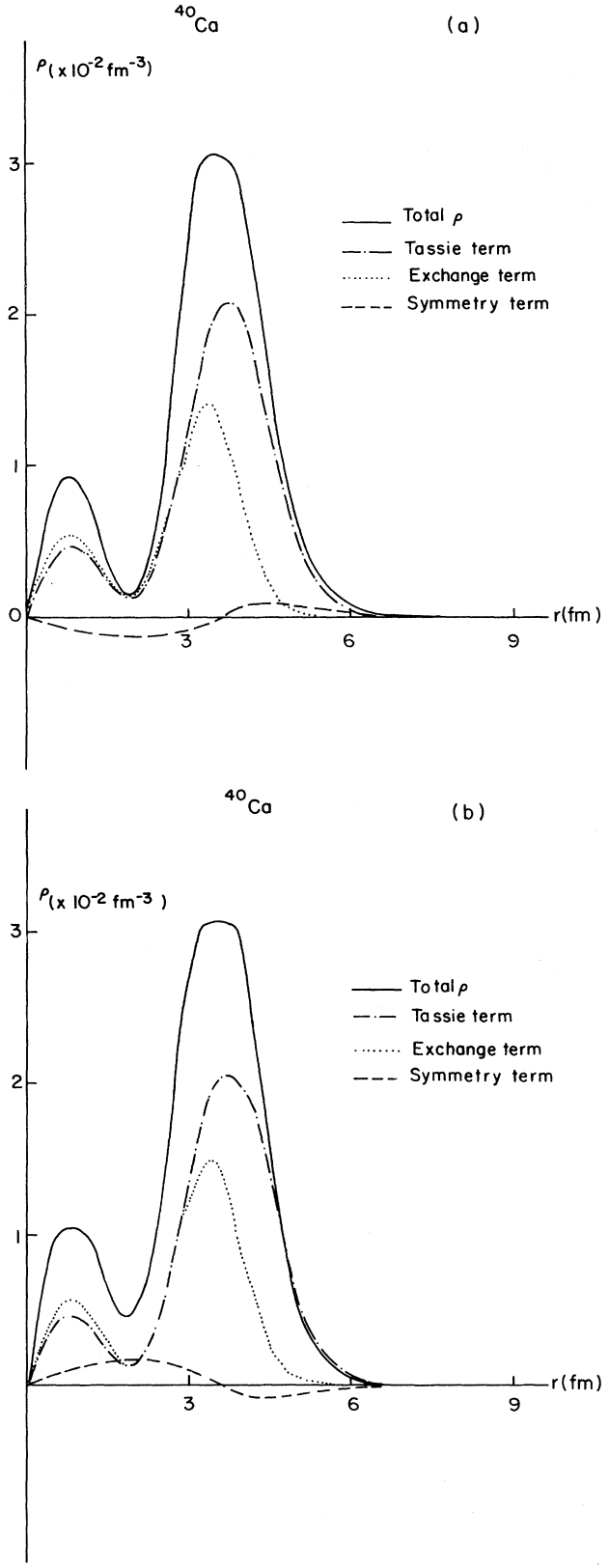

FIG. 4. The transition densities for the (a) $\Delta T_z = +1$ and (b) $\Delta T_z = -1$ modes of the dipole in ^{40}Ca, calculated using the sum-rule method.

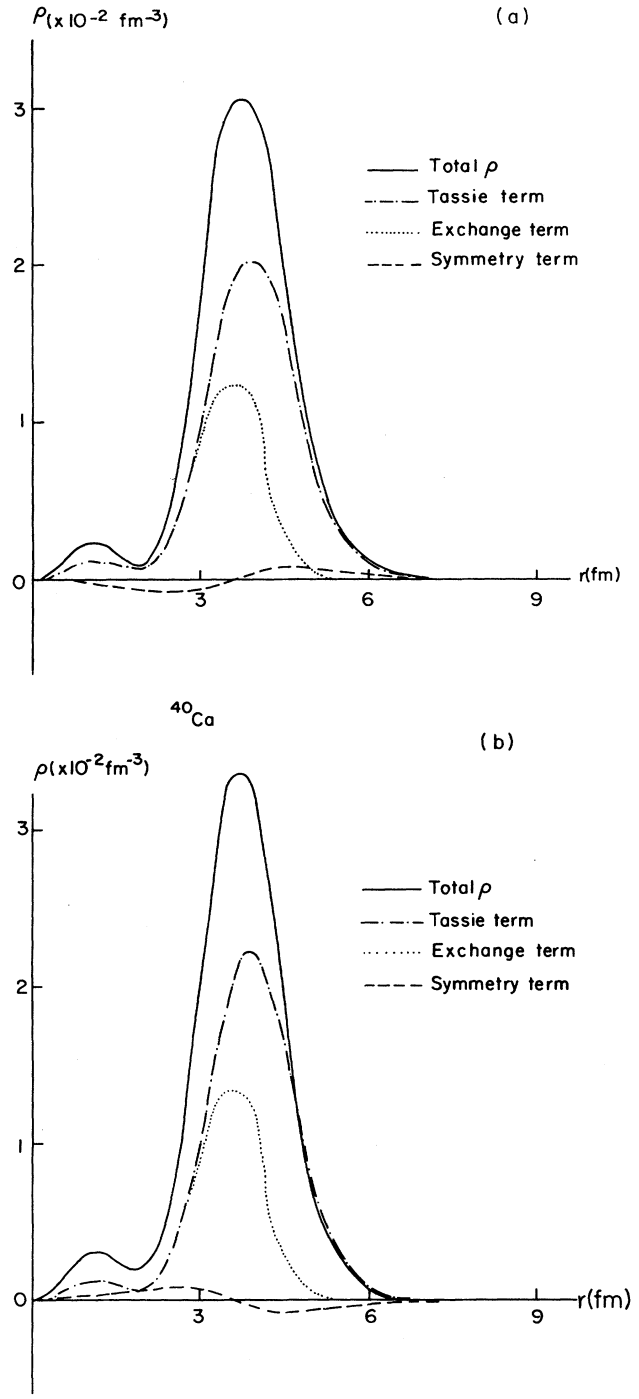

FIG. 5. The transition densities for the (a) $\Delta T_z = -1$ and (b) $\Delta T_z = -1$ modes of the quadrupole in ^{40}Ca, calculated using the sum-rule method.

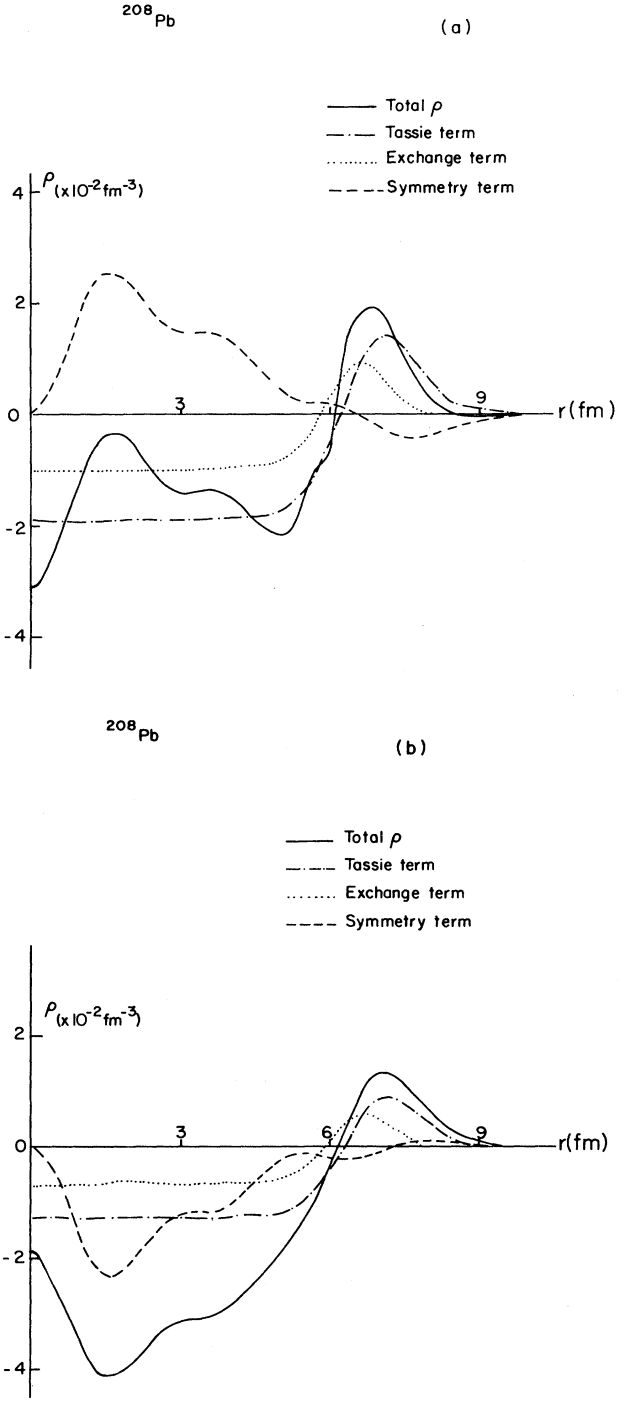

FIG. 6. The transition densities for the (a) $\Delta T_z = +1$ and (b) $\Delta T_z = -1$ modes of the monopole in ^{208}Pb, calculated using the sum-rule method.

sities are calculated using the microscopic method [Eq. (4.2)], but are normalized to the total strengths of the corresponding excitation mode, so that meaningful comparisons can be made.

We observe that, for ^{40}Ca, the transition densities for the $\Delta T_z = +1$ and $\Delta T_z = -1$ components in both the monopole and the quadrupole cases differ little. Again, this small difference is an effect of the Coulomb force. For ^{208}Pb, the transition densities for the two charge-exchange modes are very different. We should stress that

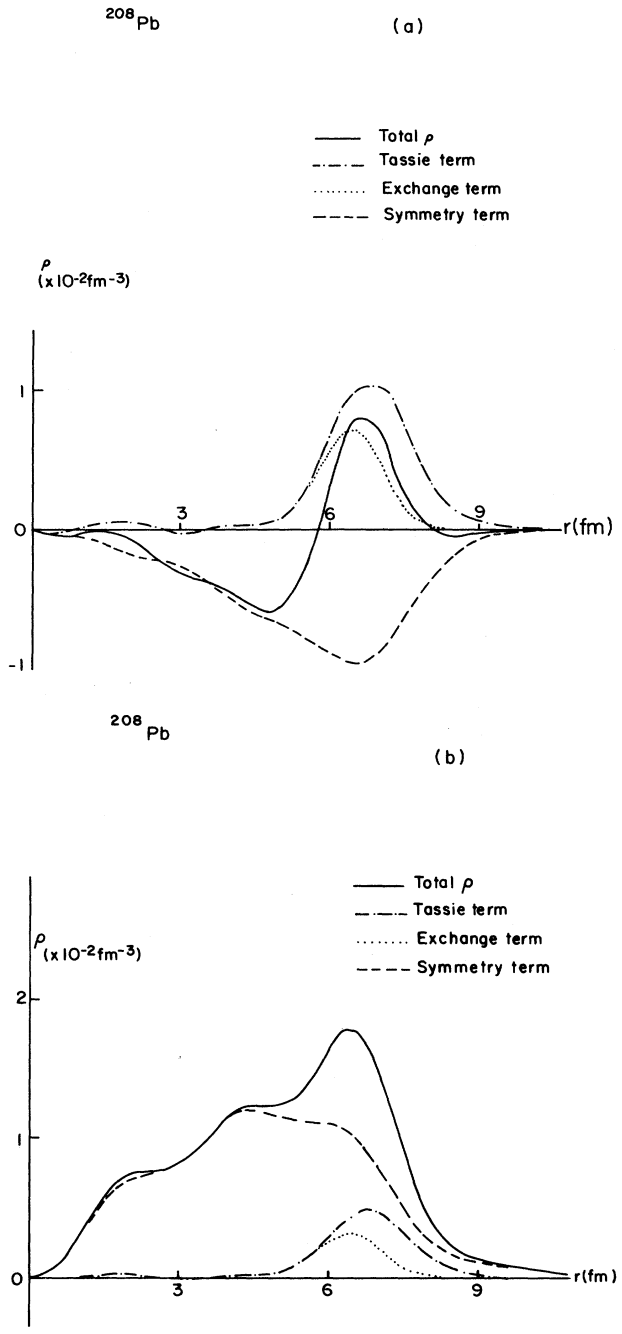

FIG. 7. The transition densities for the (a) $\Delta T_z = +1$ and (b) $\Delta T_z = -1$ modes of the dipole in ^{208}Pb, calculated using the sum-rule method.

the transition density for the $\Delta T_z = -1$ mode extends farther away from the nuclear surface than that of the $\Delta T_z = +1$ mode. This effect is due to the excess neutrons.

Finally, we should mention that the transition densities presented in Figs. 9—14 differ in their shapes from these calculated in the sum-rule approach. This is not surprising, because, in the latter approach, the closure approximation is employed, so that details of individual transi-

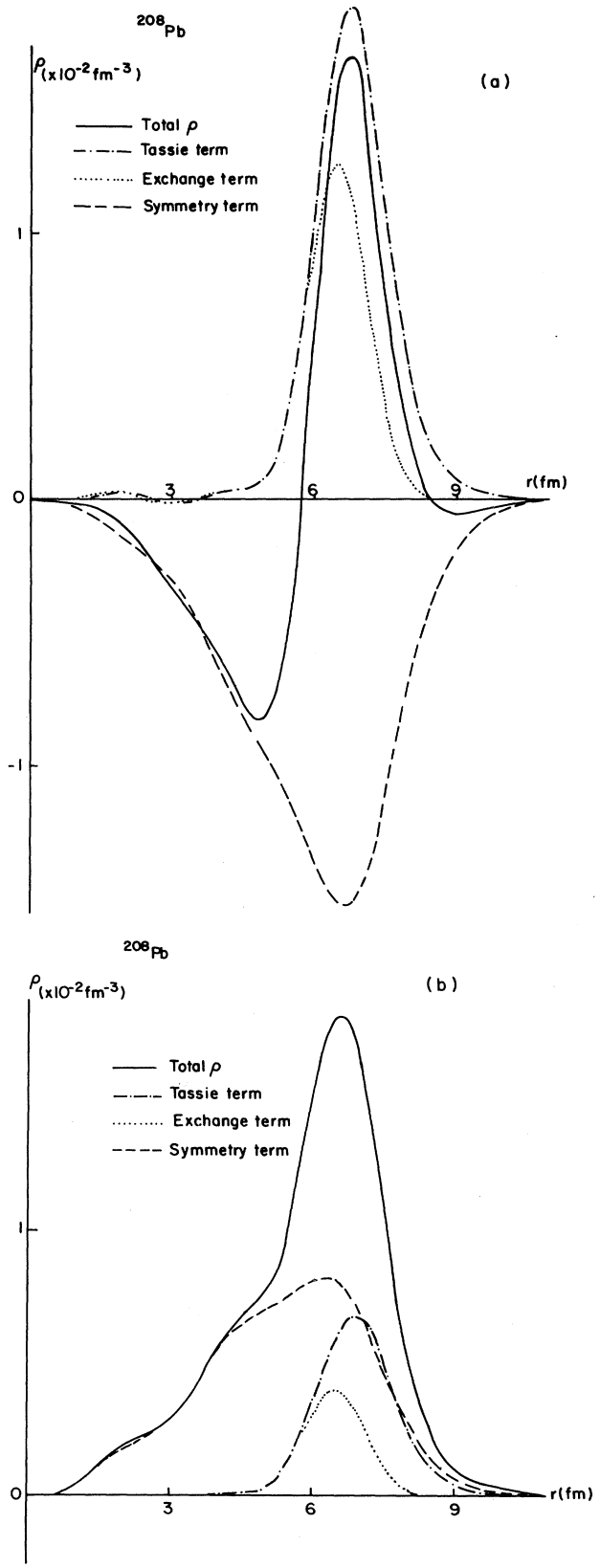

FIG. 8. The transition densities for the (a) $\Delta T_z = +1$ and (b) $\Delta T_z = -1$ modes of the quadrupole in ^{208}Pb, calculated using the sum-rule method.

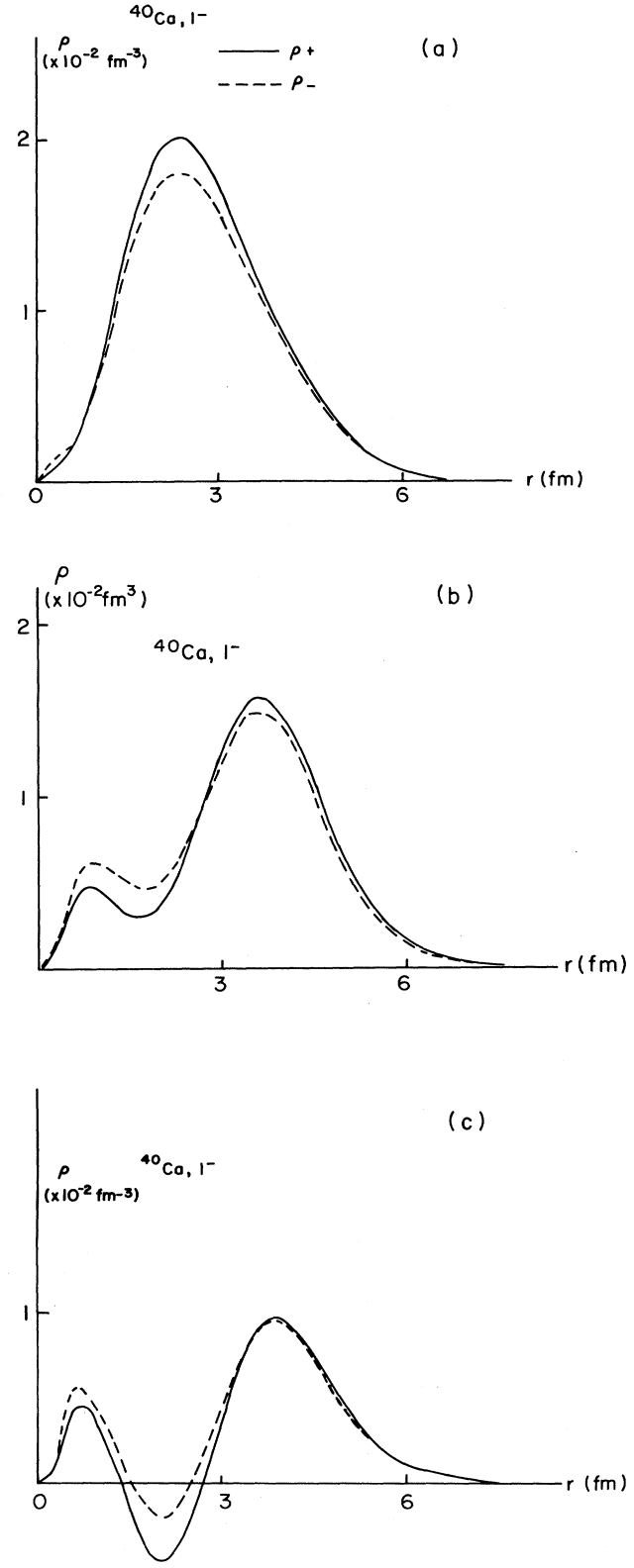

FIG. 9. The transition densities for the three strong peaks of the $\Delta T_z = +1$ dipole strength (continuous lines) and their $\Delta T_z = -1$ analogs (dashed lines) in ^{40}Ca. The transition densities are from the microscopic approach.

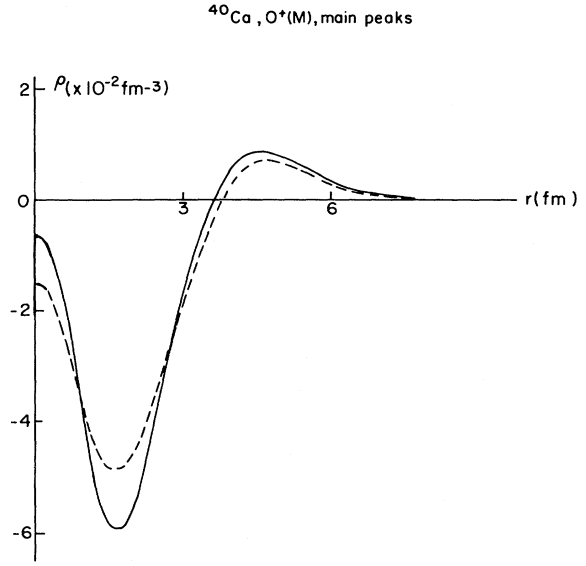

FIG. 10. The transition densities for the strongest peaks of the monopole strength in ^{40}Ca, from the microscopic approach. The continuous (dashed) line represents the transition density for the strongest peak of the $\Delta T_z = +1$ ($\Delta T_z = -1$) mode.

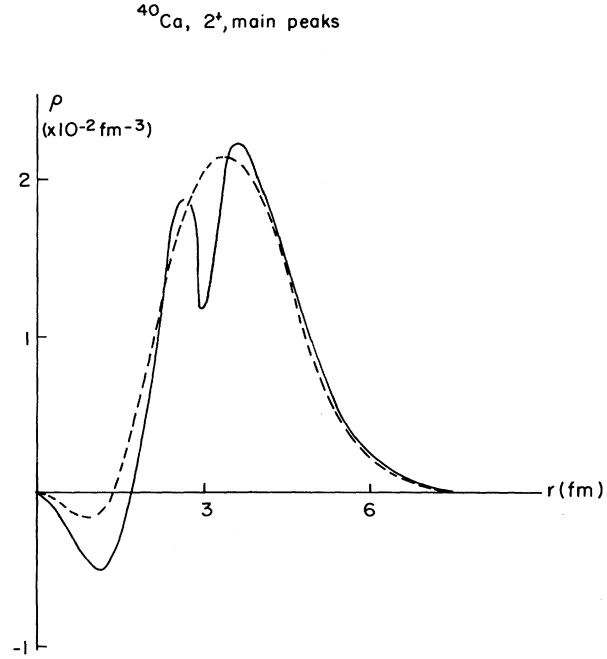

FIG. 11. The transition densities for the strongest peaks of the quadrupole strength in ^{40}Ca, from the microscopic approach. The continuous (dashed) line represents the transition density for the strongest peak of the $\Delta T_z = +1$ ($\Delta T_z = -1$) mode.

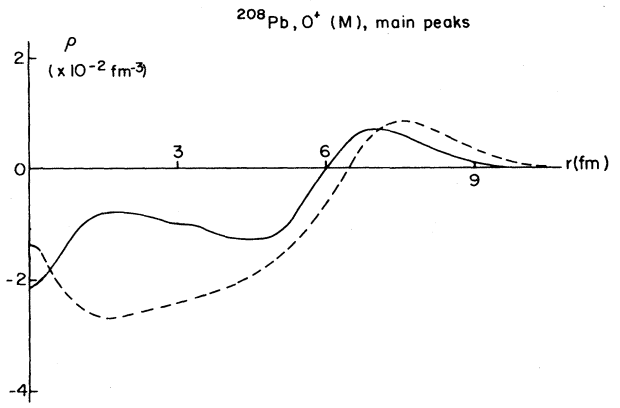

FIG. 12. The transition densities for the strongest peaks of the monopole strength in ^{208}Pb, from the microscopic approach. The continuous (dashed) line represents the transition density for the strongest peak of the $\Delta T_z = +1$ ($\Delta T_z = -1$) mode.

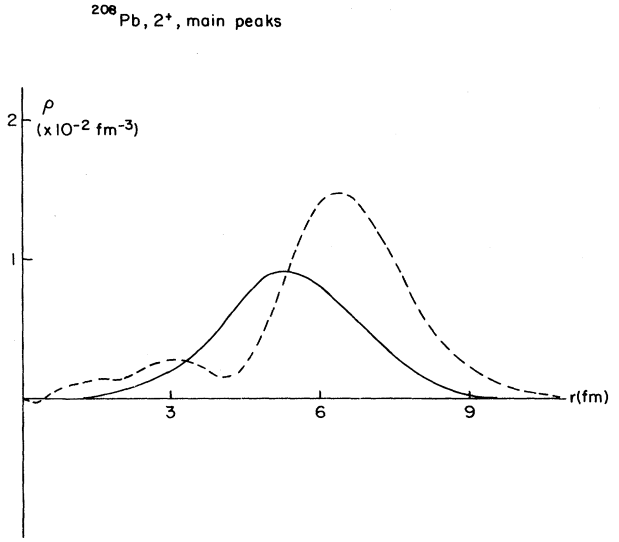

FIG. 14. The transition densities for the strongest peaks of the quadrupole strength in ^{208}Pb, from the microscopic approach. The continuous (dashed) line represents the transition density for the strongest peak of the $\Delta T_z = +1$ ($\Delta T_z = -1$) mode.

tions to various fragments of the giant states are averaged out.

V. RESULTS OF DWIA CALCULATIONS OF PION CHARGE-EXCHANGE REACTIONS

Most of the experimental data on pion charge-exchange reactions exciting giant resonances were obtained at $T_{\pi^\pm} = 165$ MeV. The absorption of the pions around the (3,3) resonance is very strong, and hence, this charge-exchange reaction is sensitive to the nuclear surface only. As we deal with the excitation of giant multipole resonances of the electric type, the appearance of the r^L factor (L is the multipolarity, and $L = 2$ in the case of the monopole) in the transition operator leads to the amplification of the effects in the outside region of the nucleus. Therefore, in pion charge-exchange reactions in the (3,3) resonance region, one can shed light on such nuclear structure effects as Coulomb polarization and the role of the excess neutrons.

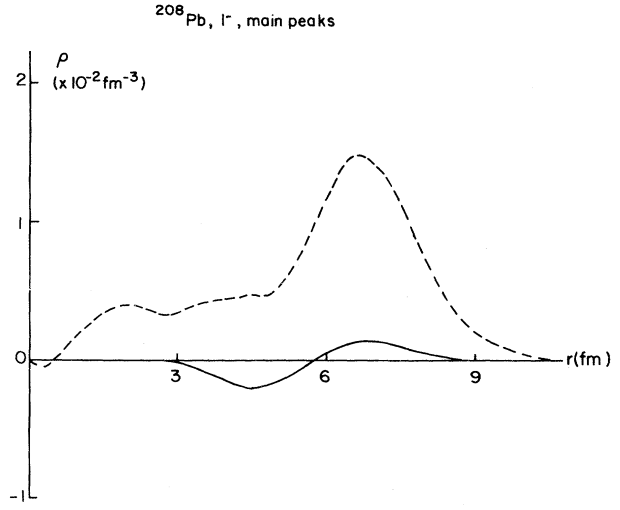

FIG. 13. The transition densities for the strongest peaks of the dipole strength in ^{208}Pb, from the microscopic approach. The continuous (dashed) line represents the transition density for the strongest peak of the $\Delta T_z = +1$ ($\Delta T_z = -1$) mode.

Correspondingly, our calculations were performed with $T_{\pi^\pm} = 165$ MeV. We used the code DWPI (Ref. 37) modified as follows: (i) external transition densities were read in and renormalized to a given strength, (ii) the coefficients of the optical potential were generated internally using pion-nucleon phase shifts from Ref. 38, (iii) HF ground state densities were used in the optical potential. The optical potential employed to distort the pionic wave functions was of the modified Kisslinger[39] form.

The results include the calculation of the cross sections using the following transition densities:

Method 1: The Tassie (macroscopic) transition density,[9] normalized to the classical oscillator EWSR.[36]

Method 2: The Tassie transition density, normalized to the calculated total RPA strength, $S_\mu^{(L)}$ of the corresponding mode.

Method 3: The transition density calculated within the sum-rule method (see Sec. III B).

Method 4: The transition density calculated within the microscopic approach (see Sec. III C).

For methods 1–3 the excitation energies used were those given in Tables II–IV. Methods 1 and 2 are introduced in order to facilitate the understanding, through comparison, of the sensitivity of $(\pi^\pm, \pi^0)$ cross sections to nuclear structure details. The nuclear structure input of method 1 contains no specific information on the nuclear response relevant to the charge-exchange process, apart from the excitation energy. The corresponding results can

tell us mainly about the differences in the cross sections due to the differing distortions in the incoming $\pi^{\pm}$ and the outgoing π^0, and differing Q values. In method 2, some information concerning the charge-exchange process is introduced in the transition densities, through the RPA strength. In methods 3 and 4 information pertaining to the charge-exchange process and to the particular features of the initial and final states is taken into account, as already described in Secs. III B and III C. Method 4 was used for the monopole and dipole of ^{40}Ca, ^{90}Zr, ^{120}Sn, and ^{208}Pb. For all other cases, in order to save computing time, we adopted the following procedure: for each peak in the RPA strength distribution, the cross sections were calculated using the average nuclear excitation energy and the average transition density for that peak. The results for each peak were afterwards summed to obtain the total angle-differential and the total angle-integrated cross sections. Tests showed that the results for each distribution

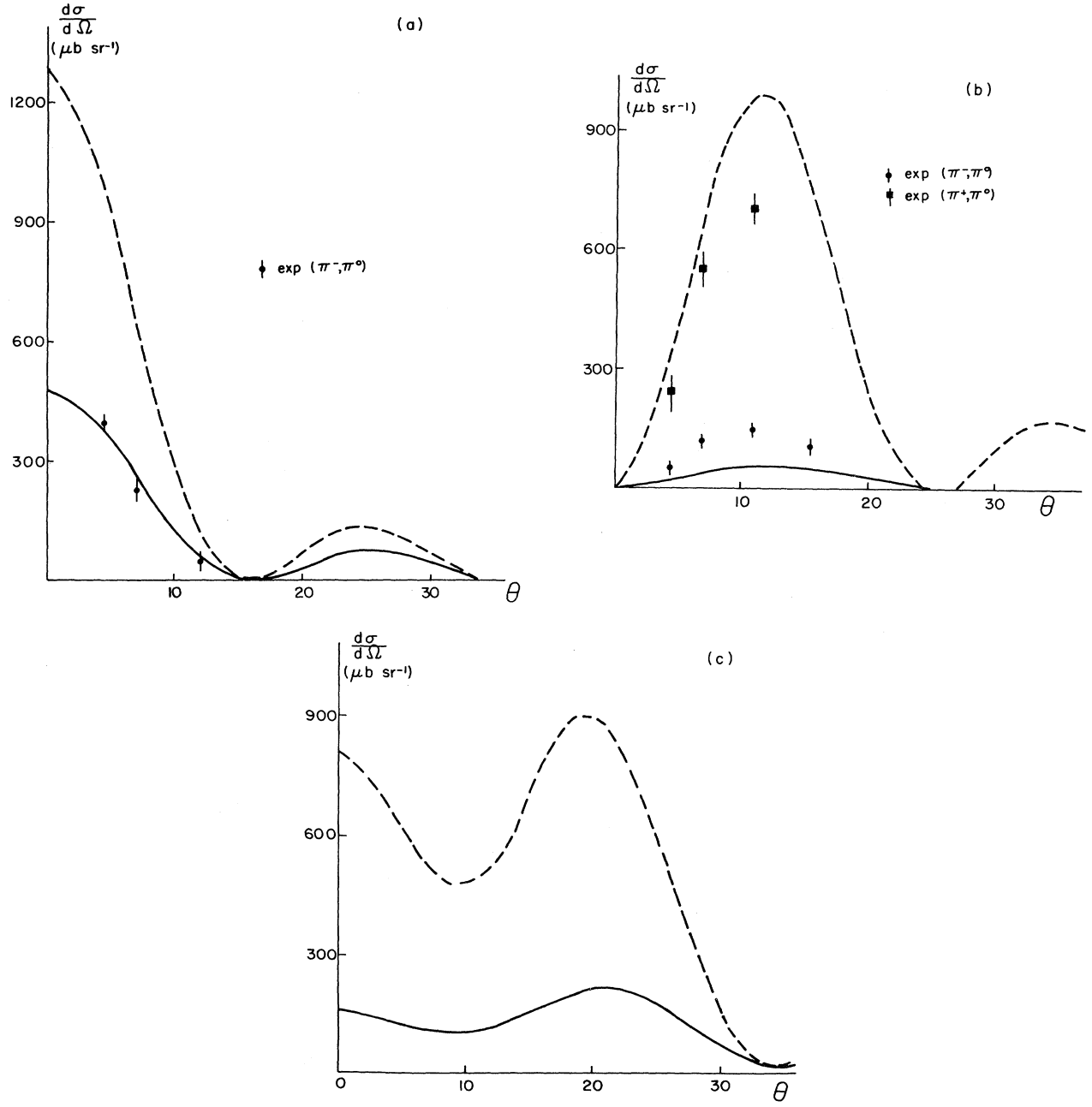

FIG. 15. The angle-differential cross sections for the (π^-,π^0) reaction (continuous lines) and the (π^+,π^0) reaction (dashed lines) exciting (a) the monopole, (b) the dipole, and (c) the quadrupole in ^{120}Sn. The results were obtained with method 3. The available experimental results are also shown.

TABLE V. The cross sections at $\theta=1°$ of the $(\pi^{\pm},\pi^0)$ reactions exciting the isovector monopole (in μb/sr).

Nucleus	Method 1		Method 2		Method 3		Method 4	
	(π^-,π^0)	(π^+,π^0)	(π^-,π^0)	(π^+,π^0)	(π^-,π^0)	(π^+,π^0)	(π^-,π^0)	(π^+,π^0)
^{40}Ca	588	499	1143	678	1183	846	1352	889
^{48}Ca	562	638	699	1171	582	1333	672	837
^{60}Ni	634	574	874	898	865	904	966	1136
^{90}Zr	726	677	1013	891	725	1088	1109	1285
^{120}Sn	780	758	660	1277	470	1238	710	2094
^{140}Ce	793	734	679	1022	435	1087	844	1615
^{208}Pb	803	752	550	1001	235	1155	562	2026

obtained by this procedure deviate by no more than 5% from results obtained in the detailed microscopic calculations.

In the framework of the response function theory, one can look upon method 4 as equivalent to a direct calculation of the nuclear response to an external perturbation, which can be represented by the operator

$$\int d^3\vec{r}\, d^3\vec{r}\,' \chi^{(-)*}(E',\vec{r}\,') \sum_{i=1}^{A} t(\vec{r},\vec{r}\,',\vec{r}_i)\chi^{(+)}(E,\vec{r}) \ .$$

A. Angular distributions

The angular distributions for each multipolarity, calculated within the four methods, have quite similar shapes. The distributions are of diffractive nature, as expected from the absorptive behavior of the charge-exchange process around the (3,3) resonance. In the limit of the strong absorption model[40,41] the angular distributions for $L=0,1$ transitions are proportional to $J_L^2(q_\perp R)$, where J_L is the Bessel function of order L, $q_\perp$ is the transverse component of the momentum transfer on the incoming pion direction, and R is a kind of effective nuclear radius,[40,42] while $L=2$ transitions are described by a combination of $J_0^2(q_\perp R)$ and $J_2^2(q_\perp R)$.

The calculated angular distributions for the charge-exchange components of the monopole attain their peak values for $\theta=0°$, then sharply decrease as θ increases. The distributions for the dipole transitions reach their maxima at angles which closely correspond to the angle at the maximum of $J_1(q_\perp R)$. The 2^+ angular distributions exhibit two maxima: the first is at $\theta=0°$ and the second one, larger in its magnitude than the first, at $\theta\approx\pi/R$ (approximately corresponding to the maximum of J_2). As examples, in Fig. 15 are shown the angular distributions for the charge-exchange reactions exciting the monopole, dipole, and quadrupole in ^{120}Sn. The results were obtained with method 3. We remark that the $\Delta T_z=+1$ angular distributions are flatter than those of the $\Delta T_z=-1$ mode corresponding to the same multipolarity. This is, of course, due to the differences in the magnitudes of the cross sections, which will be discussed below. Note, in particular, that the angular distribution of the $\Delta T_z=+1$ quadrupole is quite flat for $0°<\theta<30°$.

B. Cross sections

Tables V–VII give the calculated angle-differential cross sections for the excitation of the electric monopole, dipole, and quadrupole, respectively, for all the nuclei we treat. For the monopole we give the cross sections at $\theta=1°$ (which is close to the $\theta=0°$ maximum), for the dipole we list the cross sections at maximum, and for the quadrupole, the values of the cross sections at $\theta=1°$ (close to the $\theta=0°$ maximum) and at the second maximum are tabulated.

In method 1, only the differing Q values and the differing pionic distortions are taken into account. Large differences in Q values favor the (π^-,π^0) cross section over the (π^+,π^0) one, therefore the results obtained with method 1 satisfy $\sigma(\pi^-,\pi^0)>\sigma(\pi^+,\pi^0)$, where σ denotes the angle-differential cross section at maximum. The exception is ^{48}Ca, where the average excitation energies $E_{+1}^{(L)},E_{-1}^{(L)}$ [see Eq. (3.21)] are quite close to each other for $L=0$, 1, and 2 because the symmetry energy[36] is large as compared to the Coulomb displacement. Thus, in ^{48}Ca,

TABLE VI. The cross sections at maximum of the $(\pi^{\pm},\pi^0)$ reactions exciting the isovector dipole (in μb/sr).

Nucleus	Method 1		Method 2		Method 3		Method 4	
	(π^-,π^0)	(π^+,π^0)	(π^-,π^0)	(π^+,π^0)	(π^-,π^0)	(π^+,π^0)	(π^-,π^0)	(π^+,π^0)
^{40}Ca	712	626	935	754	846	623	1154	844
^{48}Ca	612	689	289	1312	227	1117	343	1490
^{60}Ni	709	657	499	905	335	762	543	1200
^{90}Zr	680	642	408	980	375	691	576	1099
^{120}Sn	689	665	163	1299	60	982	166	1906
^{140}Ce	654	655	56	1302	35	853	98	1482
^{208}Pb	633	634	16	1442	14	779	36	1454

TABLE VII. The cross sections at $\theta=1°$ (the upper value) and at the second maximum (the lower value) of the $(\pi^{\pm},\pi^0)$ reactions exciting the isovector quadrupole (in μb/sr).

Nucleus	Method 1		Method 2		Method 3		Method 4	
	(π^-,π^0)	(π^+,π^0)	(π^-,π^0)	(π^+,π^0)	(π^-,π^0)	(π^+,π^0)	(π^-,π^0)	(π^+,π^0)
^{40}Ca	311	263	447	330	465	349	493	348
	452	372	649	467	648	476	728	496
^{48}Ca	287	320	220	592	215	626	242	650
	396	425	303	786	305	807	346	892
^{60}Ni	335	307	353	508	348	488	365	551
	439	392	463	564	453	603	482	721
^{90}Zr	357	323	309	480	349	520	447	580
	441	388	381	577	432	607	590	706
^{120}Sn	378	371	224	697	151	792	240	1085
	459	429	272	806	211	900	297	1334
^{140}Ce	352	341	171	592	152	669	182	710
	425	370	206	643	193	751	221	791
^{208}Pb	380	358	116	687	69	732	86	810
	444	391	136	750	104	781	98	905

the pionic distortions effect overcomes the Q-value effect.

In method 2, the transition strengths [Eq. (3.20)] are also introduced, in addition to the effects already taken into account in method 1. For $N>Z$ nuclei, the excess neutrons are responsible for the fact that the strength in the $\Delta T_z=-1$ mode is larger than that in the $\Delta T_z=+1$ mode. Therefore, one should expect that the cross sections, as calculated with method 2, obey $\sigma(\pi^-,\pi^0)<\sigma(\pi^+,\pi^0)$, even though the Q-value effect favors $\sigma(\pi^+,\pi^0)$. In ^{40}Ca, where $N=Z$, the cross sections calculated with method 2 obey $\sigma(\pi^-,\pi^0)>\sigma(\pi^+,\pi^0)$ due to the following two reasons: (i) the above mentioned Q-value effect, and (ii) the Coulomb polarization effect.

In the realistic calculations, performed with methods 3 and 4, in addition to the factors discussed in relation to methods 1 and 2, the *particular shapes* of the transition densities in the two $\Delta T_z=+1$ and $\Delta T_z=-1$ modes also have an effect on the values of the resulting cross sections. In method 4, the Q-value effects and the changes occurring in the transition densities, as one goes to different nuclear excitations energies, are taken into account. Therefore, it is not surprising that the absolute values of the cross sections calculated with methods 3 and 4 differ considerably. However, the ratios of the cross sections for the two charge exchange components ($\Delta T_z=\pm1$) of the same multipolarity, as calculated in both method 3 and method 4, are in reasonable agreement with each other.

As shown in Secs. III B and III C, the shapes of the transition densities calculated within the sum-rule method and the microscopic approach are affected by the differences in the neutron and proton densities, resulting from the Coulomb polarization of the core protons, and by the distribution of the excess neutrons. As explained at the beginning of this section, one expects these effects to be amplified in pion charge exchange reactions around the (3,3) resonance. Therefore, the cross sections calculated with methods 3 and 4 should reflect this kind of amplification. For example, calculations with methods 3 and 4 yield for $\sigma(\pi^-,\pi^0)/\sigma(\pi^+,\pi^0)$ for the charge-exchange dipole in ^{40}Ca the values 1.36 and 1.37, respectively. This ratio is significantly larger than the value obtained due to the Q value and distortion effects (method 1) only,

$$\sigma(\pi^-,\pi^0)/\sigma(\pi^+,\pi^0)=1.14\ ,$$

and larger than the value obtained with method 2,

$$\sigma(\pi^-,\pi^0)/\sigma(\pi^+,\pi^0)=1.24\ .$$

In ^{40}Ca, the Coulomb polarization effect results in $\sigma(\pi^-,\pi^0)>\sigma(\pi^+,\pi^0)$ also for $L=0$, 2 with both methods 3 and 4. For the $N>Z$ nuclei, the excess neutrons, which cause the $\Delta T_z=-1$ mode transition densities to extend farther away from the nuclear surface than those of the $\Delta T_z=+1$ mode, favor the (π^+,π^0) cross section over the (π^-,π^0) one. Note that, for the monopole of ^{90}Zr, the cross sections of the two components are close to each other although $N-Z=10$ for this nucleus: the effect of the excess neutrons is reduced greatly by the Coulomb polarization of the core protons.

We will give more details on the microscopic calculations with method 4. As opposed to methods 1, 2, and 3, where only the angle-differential cross section for a single state is calculated, in method 4 one obtains the double differential cross section $d^2\sigma/d\Omega\, dE_{n_\mu}$, where E_{n_μ} is the excitation energy of the state $|n_\mu\rangle$, $\mu=\pm1$. The total angle-differential cross section is calculated as follows:

$$\frac{d\sigma}{d\Omega}=\int_0^\infty \frac{d^2\sigma}{d\Omega\, dE_{n_\mu}} dE_{n_\mu} . \tag{5.1}$$

We also introduce the average reaction excitation energy, ϵ_μ, defined as

$$\epsilon_\mu=\frac{\int_0^\infty E_{n_\mu}\frac{d^2\sigma}{d\Omega\, dE_{n_\mu}} dE_{n_\mu}}{\frac{d\sigma}{d\Omega}} . \tag{5.2}$$

This quantity may be compared with the experimentally measured average energies. The quantities ϵ_μ, E_μ may differ, sometimes by as much as 4 MeV. For the (π^+,π^0) reaction exciting the monopole in ^{90}Zr, the RPA excitation energy is 42.3 MeV (see Table II) and the average reaction excitation energy is 38.1 MeV. Another example is the case of the (π^-,π^0) reaction exciting the dipole in ^{120}Sn: we obtained $E_{+1}=6.5$ MeV and $\epsilon_{+1}=7.9$ MeV. The reason for these differences is provided by the fact that the pion-nucleus transition operator, as opposed to the operators considered in RPA, is *energy dependent.* This energy dependence enters in a complicated way through the pionic distortions and through the pion-nucleon t matrix.

In Figs. 16–23, we show the calculated double-differential cross sections, at the angles corresponding to their maxima, for the monopole and dipole of ^{40}Ca, ^{90}Zr, ^{120}Sn, and ^{208}Pb. Note that due to the above-mentioned energy dependence, these distributions differ visibly from the RPA ones obtained with the multipole operators as

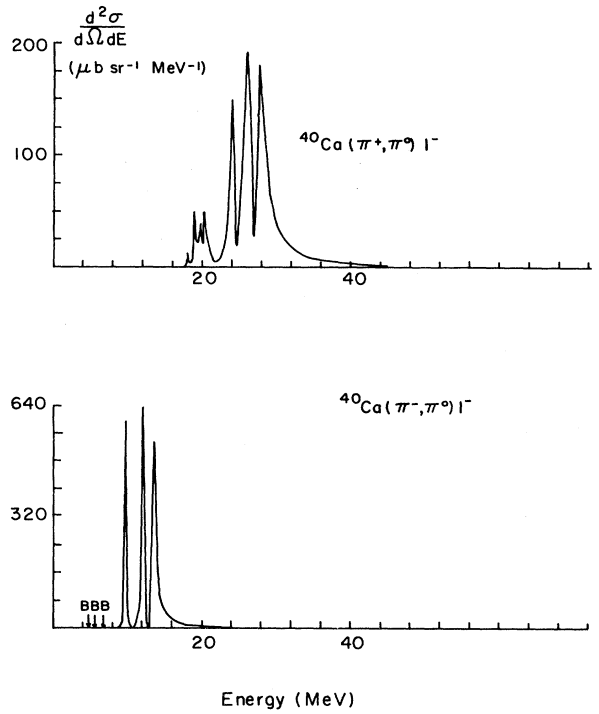

FIG. 17. The calculated double-differential cross sections, at the angles corresponding to their maxima, of the $(\pi^\pm,\pi^0)$ reactions exciting the dipole of ^{40}Ca. The cross sections are plotted as a function of the nuclear excitation energy with respect to the target ground state.

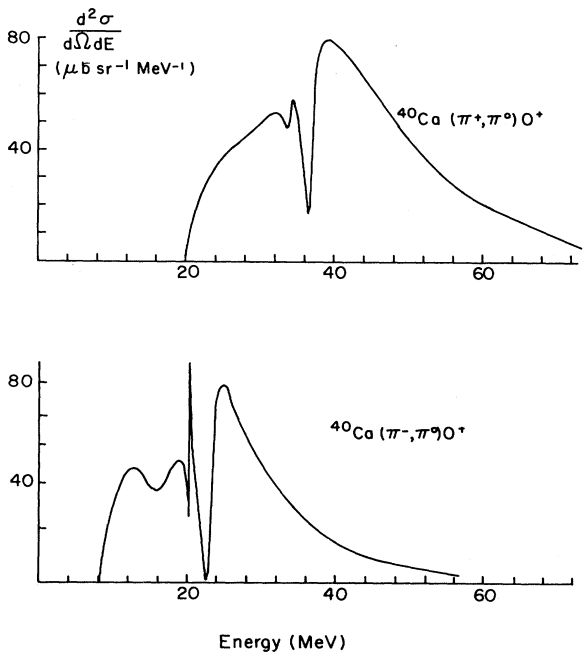

FIG. 16. The calculated double-differential cross sections, at the angles corresponding to their maxima, of the $(\pi^\pm,\pi^0)$ reactions exciting the monopole of ^{40}Ca. The cross sections are plotted as a function of the nuclear excitation energy with respect to the target ground state.

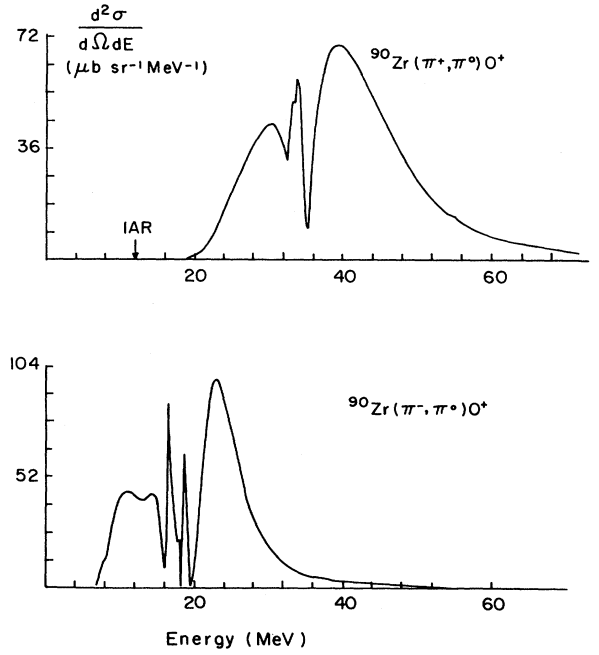

FIG. 18. The calculated double-differential cross sections, at the angles corresponding to their maxima, of the $(\pi^\pm,\pi^0)$ reactions exciting the monopole of ^{90}Zr. The cross sections are plotted as a function of the nuclear excitation energy with respect to the target ground state.

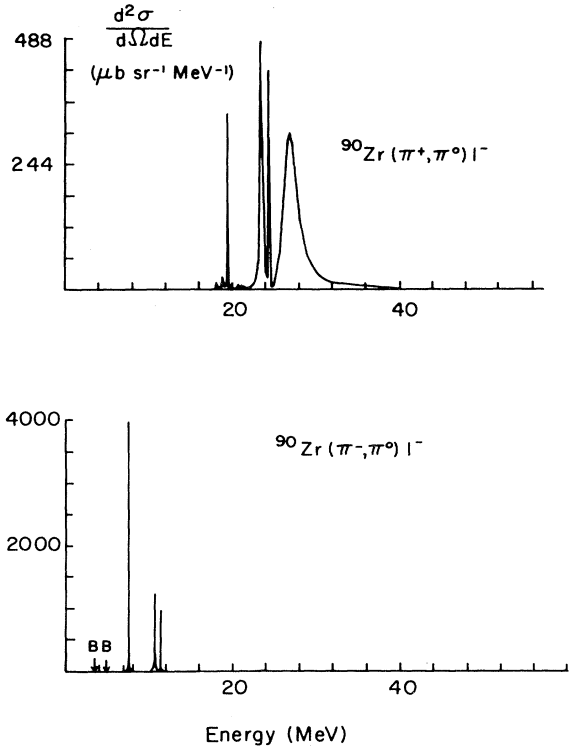

FIG. 19. The calculated double-differential cross sections, at the angles corresponding to their maxima, of the $(\pi^{\pm},\pi^0)$ reactions exciting the dipole of ^{90}Zr. The cross sections are plotted as a function of the nuclear excitation energy with respect to the target ground state.

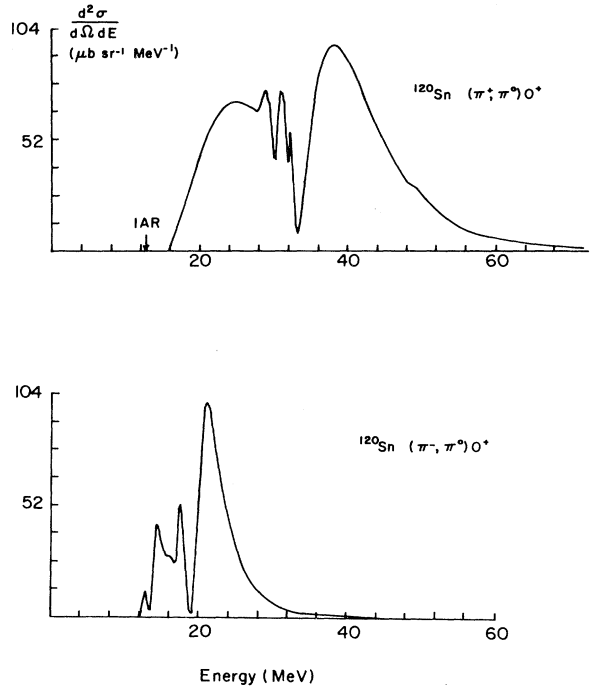

FIG. 20. The calculated double-differential cross sections, at the angles corresponding to their maxima, of the $(\pi^{\pm},\pi^0)$ reactions exciting the monopole of ^{120}Sn. The cross sections are plotted as a function of the nuclear excitation energy with respect to the target ground state.

probes (see Figs. 1 and 2 in this work and figures in Ref. 7). Also, the difference in the space dependences of the multipole operator and the pion-nucleus interaction might contribute to the changes in the distributions. The widths of the individual peaks in Figs. 16–23 correspond to particle escape widths. For example, the monopole transitions in the $\Delta T_z=-1$ channel exhibit a wide peak at the high energy end with a width ranging from about 10 to 15 MeV. In the $\Delta T_z=+1$, these widths are lower, because lower energies correspond to smaller penetrability factors. The introduction of a relatively small spreading width[33] will smooth out the fragmentation in the $\Delta T_z=+1$ mode.

C. Comparison with experiment

Experimental results concerning the observation of the charge-exchange components of the isovector dipole and monopole in $(\pi^{\pm},\pi^0)$ reactions became recently available.[4,5] In Refs. 4 and 5 the authors used incoming pions with $T_{\pi^{\pm}}=165$ MeV, to study the excitation of giant resonances in a variety of nuclei. The outgoing pion energies and directions were measured using the Los Alamos Meson Physics Facility (LAMPF) π^0 spectrometer. The quantitative analysis was performed under the assumption that the background was isotropic, and therefore could be subtracted out. The angular distributions were extracted by a least square fit procedure. The orbital angular momentum transfer was inferred from the measured angle-differential cross sections by comparing them with the results of DWIA calculations.

To begin with, we find that the shapes of the angular distributions, as calculated with methods 1–4, are in satisfactory agreement with the shapes of experimental ones. This agreement is exemplified in Fig. 15, where the available experimental $d\sigma/d\Omega$ are also drawn. Note that the absolute values of the angular distributions in Fig. 15 are not normalized to experiment. Therefore, the apparent discrepancy results mainly from the discrepancy in the absolute value.

We will now discuss the magnitudes of the calculated cross sections and the average excitation energies, as compared to experiment.

1. The charge exchange dipole

The measured cross sections at maximum in the cross sections for ^{40}Ca are the following[4]:

$$\sigma(\pi^-,\pi^0)=0.87\pm0.09 \text{ mb/sr} ,$$

$$\sigma(\pi^-,\pi^0)=0.51\pm0.05 \text{ mb/sr} ,$$

and

$$\sigma(\pi^-,\pi^0)/\sigma(\pi^+,\pi^0)=1.69\pm0.24 .$$

The results for the absolute values of the cross sections, obtained with the realistic methods 3 and 4, agree reason-

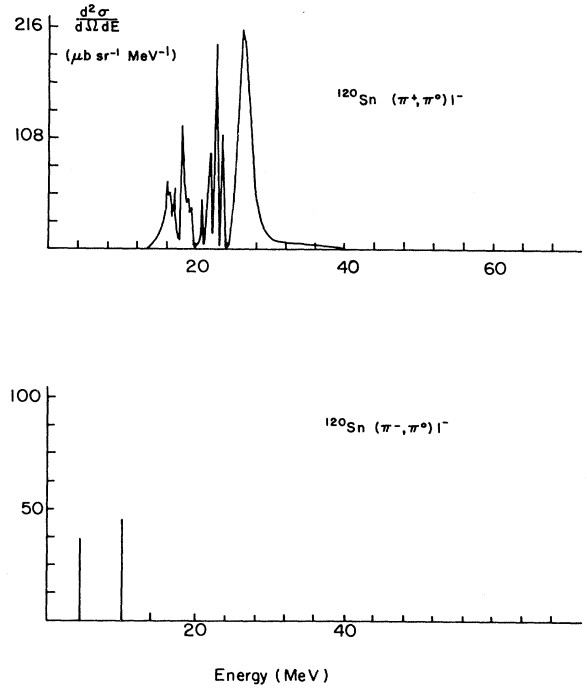

FIG. 21. The calculated double-differential cross sections, at the angles corresponding to their maxima, of the $(\pi^{\pm},\pi^0)$ reactions exciting the dipole of ^{120}Sn. The cross sections are plotted as a function of the nuclear excitation energy with respect to the target ground state.

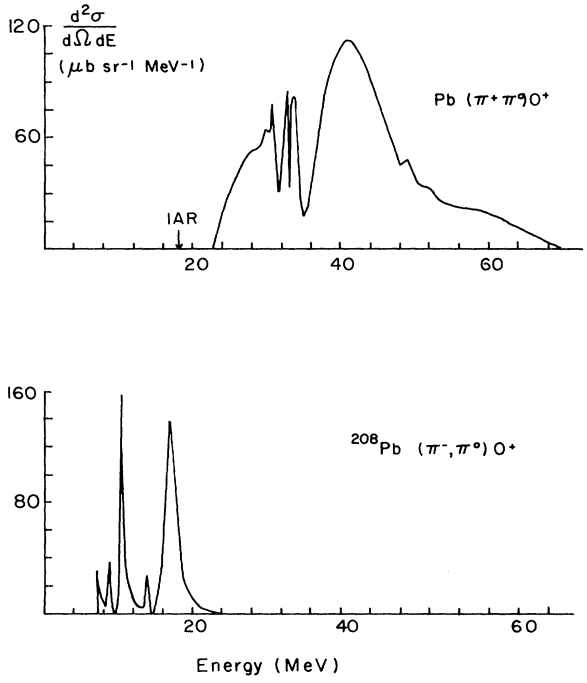

FIG. 22. The calculated double-differential cross sections, at the angles corresponding to their maxima, of the $(\pi^{\pm},\pi^0)$ reactions exciting the monopole of ^{208}Pb. The cross sections are plotted as a function of the nuclear excitation energy with respect to the target ground state.

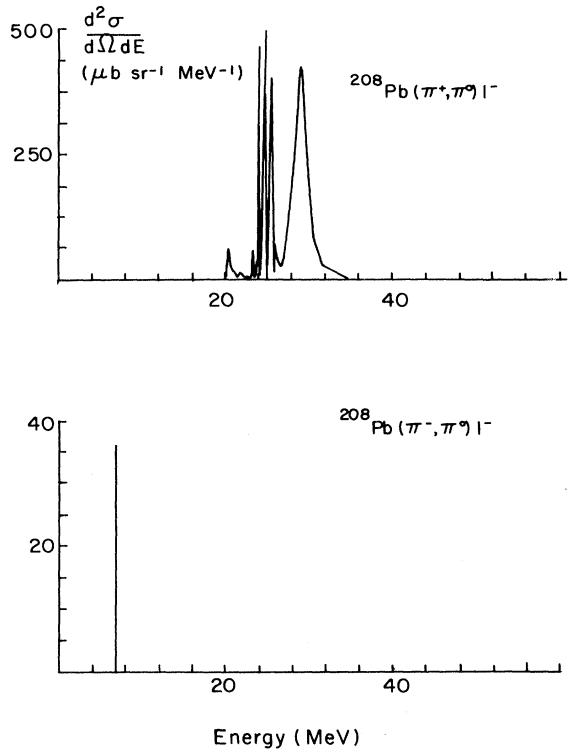

FIG. 23. The calculated double-differential cross sections, at the angles corresponding to their maxima, of the $(\pi^{\pm},\pi^0)$ reactions exciting the dipole of ^{208}Pb. The cross sections are plotted as a function of the nuclear excitation energy with respect to the target ground state.

ably well with experiment. In particular, method 3 yields cross sections which are very close to the experimental ones. The theoretical ratio is about 1.4 in methods 3 and 4 while methods 1 and 2 yield for this ratio the values 1.14 and 1.24, respectively. Thus, when Coulomb polarization effects in the initial and final nuclei are taken into account in a detailed manner, the calculated ratio of the cross sections at their maxima is closer to experiment.

The $\Delta T_z = +1$ component of the isovector dipole in ^{90}Zr was observed[5] at an excitation energy[43] of 9.0 ± 0.7 MeV with respect to the target nucleus ground state. The calculated RPA excitation energy is 8.2 MeV, and the reaction average energy is $\epsilon_{+1}=8.0$ MeV. The cross sections at the maximum obtained with methods 3 and 4 are in agreement with experiment.

In ^{120}Sn, there is data[5] on both charge exchange components of the dipole. The $\Delta T_z = +1$ component was observed at 7.8 ± 0.85 MeV above the ^{120}Sn target ground state. The RPA energy is 6.5 MeV, and the average reaction energy is 7.9 MeV. The $\Delta T_z = -1$ component was reported at 24.1 ± 1.2 MeV. The RPA calculations yield 25.6 MeV, and the reaction average excitation energy is 24.5 MeV. We see that DWIA calculations, where the energy dependence of the operator which excites the dipole is taken into account, yield results which compare well with experiment for both the $\Delta T_z = +1$ and $\Delta T_z = -1$ modes in ^{120}Sn.

The experimentally measured magnitudes of the cross sections are

$$\sigma(\pi^-,\pi^0)=154\pm32\ \mu\text{b/sr}$$

and

$$\sigma(\pi^+,\pi^0)=704\pm151\ \mu\text{b/sr}\ .$$

The theoretical magnitudes are

$$\sigma(\pi^-,\pi^0)=60\ \mu\text{b/sr (method 3)}\ ,$$
$$=166\ \mu\text{b/sr (method 4)}\ ,$$
$$\sigma(\pi^+,\pi^0)=982\ \mu\text{b/sr (method 3)}$$
$$=1906\ \mu\text{b/sr (method 4)}\ .$$

The calculated ratios $\sigma(\pi^+,\pi^0)/\sigma(\pi^-,\pi^0)$ are 16.4 in method 3 and 11.5 in method 4, while the experimental value is 4.7. This shows that the influence of the excess neutrons in the charge-exchange dipole of ^{120}Sn is overestimated in our calculations, as compared to experiment.

2. *The charge-exchange monopole*

The $\Delta T_z=+1$ component of the isovector monopole in ^{90}Zr was observed[5] at 22.8 ± 1.3 MeV. The theoretical results are the following: 22.9 MeV in RPA and 21.9 MeV with method 4. The experimental cross section at the maximum was found to be 891 ± 125 μb/sr. The theoretical results agree with this value.

In ^{120}Sn, a $\Delta T_z=+1$ transition of 0^+ multipolarity was observed[5] in the (π^-,π^0) reaction, at 18.3 ± 0.5 MeV. The theoretical excitation energies are somewhat larger: 22.4 MeV from RPA calculations, and 23.9 MeV from method 4. The cross sections calculated with methods 3 and 4 are in good agreement with experiment. In Ref. 5, the authors also quote a tentative result for the cross section of the (π^+,π^0) reaction exciting the monopole in ^{120}Sn. These results lead to a value of $\sigma(\pi^-,\pi^0)/\sigma(\pi^+,\pi^0)$ which is larger than 1, in disagreement with the theoretical estimate:

$$\sigma(\pi^-,\pi^0)/\sigma(\pi^+,\pi^0)=0.37$$

in method 3, and 0.34 in method 4.

Preliminary experimental results[44] indicate that a lower limit for the ratio $\sigma(\pi^-,\pi^0)/\sigma(\pi^+,\pi^0)$ for the monopole of ^{40}Ca is about 2. The theoretical predictions are

$$\sigma(\pi^-,\pi^0)/\sigma(\pi^+,\pi^0)=1.40$$

in method 3 and 1.52 in method 4.

3. *The charge-exchange quadrupole*

To date, the $\Delta T_z=+1$ components of the isovector quadrupole have not been observed. Theoretically, $(\pi^\pm,\pi^0)$ reactions exciting the quadrupole have substantial cross sections (about 30—80 % of the monopole cross sections). For example, the $\Delta T_z=+1$ component of the quadrupole in ^{120}Sn is theoretically found to be at 18.6 MeV, and its forward angle cross section is about one-third of the monopole one.

The relative flatness of the calculated angular distributions for the (π^-,π^0) reactions [see Fig. 15(c)] suggests that some of the quadrupole strength might be "hidden" in the background, and, therefore subtracted out in the experimental analysis.

VI. SUMMARY

In this work, we presented the results of a systematic study of pion charge-exchange reactions in which giant electric isovector resonances are excited. We use the DWIA framework and we emphasized the nuclear structure aspects which are probed in these reactions. The self-consistent HF-RPA framework was employed and distributions of strength, excitation energies, and transition densities were derived. The cross section calculations were performed using four methods. The description of the various relevant aspects of nuclear structure was improved from method to method. We found that the calculated absolute values of the cross sections and their ratios are sensitive to details of the nuclear structure.

The theoretical results for the cross sections and average energies are in reasonable agreement with the available experimental results. More experimental data, including the one whose analysis is still in progress, will make the comparison with theory even more significant.

In conclusion, this work shows that pion charge exchange reactions, along with other reactions, are a useful tool in the study of giant resonances in nuclei. In particular, because of the three charge states of the pion, we can learn about the isovector properties of giant resonances, such as isospin structure, relative transition strengths of the various charge exchange components, and shapes of the transition densities and their relation to the isovector part of the ground state density.

ACKNOWLEDGMENTS

We wish to thank Dr. J. Alster, Dr. H. W. Baer, Dr. J. D. Bowman, Dr. A. Erell, Dr. M. B. Johnson, and Dr. E. R. Siciliano for helpful discussions. This work was supported by the U.S. Department of Energy and the U.S.-Israel Binational Science Foundation.

[1]E. C. Bartels and A. K. Kerman, MIT Report 2098-286, 1966; G. A. Miller and J. E. Spencer, Ann. Phys. (N.Y.) 100, 562 (1976); N. Auerbach and J. Warszawski, Phys. Lett. 45B, 171 (1973).

[2]J. Alster and J. Warszawski, Phys. Rep. 52C, 87 (1979); H. W. Baer *et al.*, Phys. Rev. Lett. 45, 982 (1980).

[3]H. W. Baer *et al.*, Nucl. Instrum. Methods 180, 445 (1981).

[4]H. W. Baer *et al.*, Phys. Rev. Lett. 49, 1376 (1982).

[5]J. D. Bowman *et al.*, Phys. Rev. Lett. 50, 1195 (1983).

[6]N. Auerbach, Phys. Rev. Lett. 49, 913 (1982).

[7]N. Auerbach and Amir Klein, Nucl. Phys. A395, 77 (1983).

[8]J. M. Eisenberg and D. S. Koltun, *The Theory of Meson Interactions with Nuclei* (Wiley, New York, 1980).

[9]L. J. Tassie, Aust. J. Phys. 9, 407 (1956).

[10]M. Goldhaber and E. Teller, Phys. Rev. 74, 1046 (1948).
[11]H. Steinwedel, J. Jensen, and P. Jensen, Phys. Rev. 79, 1019 (1950).
[12]J. D. Walecka, Phys. Rev. 126, 653 (1962).
[13]C. Werntz and H. Überall, Phys. Rev. 149, 762 (1966).
[14]N. Auerbach, Phys. Lett. 36B, 293 (1971).
[15]T. J. Deal and S. Fallieros, Phys. Rev. C 7, 1709 (1973).
[16]J. V. Noble, Phys. Rep. 40C, 241 (1978).
[17]T. Suzuki, Phys. Lett. 83B, 147 (1979).
[18]W. Theiss and E. Werner, Phys. Lett. 44B, 481 (1973).
[19]G. F. Bertsch and S. F. Tsai, Phys. Rep. 18C, 125 (1975).
[20]K. F. Liu and G. E. Brown, Nucl. Phys. A265, 385 (1976).
[21]G. A. Rinker and J. Speth, Nucl. Phys. A306, 360 (1978).
[22]J. P. Blaizot, Phys. Rep. 64C, 172 (1980).
[23]V. Bernard and Nguyen Van Giai, Nucl. Phys. A348, 75 (1980).
[24]G. F. Bertsch, D. Cha, and H. Toki, Phys. Rev. C 24, 533 (1981).
[25]N. Auerbach, L. Zamick, and Amir Klein, Phys. Lett. 118B, 256 (1982).
[26]Nguyen Van Giai, N. Auerbach, and A. Z. Mekjian, Phys. Rev. Lett. 46, 1944 (1981); N. Auerbach and A. Klein, Phys. Lett. 114B, 95 (1982).
[27]D. J. Thouless, *The Quantum Mechanics of Many Body Problems* (Academic, New York, 1961).
[28]N. Auerbach and Amir Klein, Phys. Rev. C 27, 1818 (1983).
[29]M. Beiner *et al.*, Nucl. Phys. A228, 29 (1975).
[30]N. Auerbach and Nguyen Van Giai, Phys. Rev. C 24, 782 (1981).
[31]A. G. Courtney and J. D. Fox, At. Data Nucl. Data Tables, 15, 141 (1975).
[32]S. Shlomo and G. F. Bertsch, Nucl. Phys. A243, 507 (1975).
[33]S. Adachi and N. Auerbach, Phys. Lett. (in press).
[34]E. H. Auerbach, S. Kahana, and J. Weneser, Phys. Rev. Lett. 23, 1253 (1969).
[35]L. Zamick, Phys. Lett. 39B, 421 (1972).
[36]A. Bohr and B. R. Mottelson, *Nuclear Structure* (Benjamin, New York, 1975), Vol. II.
[37]R. A. Eisenstein and G. A. Miller, Comput. Phys. Commun. 11, 95 (1976).
[38]G. Rowe, M. Salomon, and R. H. Landau, Phys. Rev. C 18, 584 (1978).
[39]L. S. Kisslinger and F. Tabakin, Phys. Rev. C 9, 188 (1974).
[40]M. B. Johnson, Phys. Rev. C 22, 192 (1980).
[41]A. Gal, Phys. Rev. C 25, 2680 (1982).
[42]J. D. Bowman, M. B. Johnson, and J. W. Negele, Phys. Rev. Lett. 46, 1614 (1981).
[43]In Refs. 4 and 5 the authors include the neutron proton mass differences in the values given for the average excitation energies. Thus, in order to be able to compare with our results, we will subtract the above-mentioned quantity from the experimental average energies corresponding to (π^-,π^0) reactions, and add it to those corresponding to (π^+,π^0) reactions.
[44]J. D. Bowman (private communication).